AGU PUBLICATIONS

JGR

Journal of Geophysical Research: Oceans

RESEARCH ARTICLE

10.1002/2015JC011047

Southern Ocean eddy phenomenology

I. Frenger[1,2,3], M. Münnich[1], N. Gruber[1,2], and R. Knutti[4]

[1]Environmental Physics, Institute of Biogeochemistry and Pollutant Dynamics, ETH Zurich, Zurich, Switzerland, [2]Center for Climate Systems Modeling, ETH Zurich, Zurich, Switzerland, [3]Now at Program in Atmospheric and Oceanic Sciences, Princeton University, Princeton, New Jersey, USA, [4]Climate Physics, Institute of Atmospheric and Climate Science, ETH Zurich, Zurich, Switzerland

Key Points:
- Southern Ocean mesoscale eddy characteristics analyzed based on satellite and profiling float data
- Spatial variation of anticyclonic and cyclonic eddy numbers and characteristics
- Intimate link of eddies and topography

Supporting Information:
- Supporting Information S1

Correspondence to:
I. Frenger,
ifrenger@princeton.edu

Citation:
Frenger, I., M. Münnich, N. Gruber, and R. Knutti (2015), Southern Ocean eddy phenomenology, *J. Geophys. Res. Oceans*, *120*, 7413–7449, doi:10.1002/2015JC011047.

Received 14 JUN 2015
Accepted 16 OCT 2015
Accepted article online 23 OCT 2015
Published online 18 NOV 2015
Corrected 20 JAN 2017

This article was corrected on 20 JAN 2017. See the end of the full text for details.

Abstract Mesoscale eddies are ubiquitous features in the Southern Ocean, yet their phenomenology is not well quantified. To tackle this task, we use satellite observations of sea level anomalies and sea surface temperature (SST) as well as in situ temperature and salinity measurements from profiling floats. Over the period 1997–2010, we identified over a million mesoscale eddy instances and were able to track about 10^5 of them over 1 month or more. The Antarctic Circumpolar Current (ACC), the boundary current systems, and the regions where they interact are hot spots of eddy presence, representing also the birth places and graveyards of most eddies. These hot spots contrast strongly to areas shallower than about 2000 m, where mesoscale eddies are essentially absent, likely due to topographical steering. Anticyclones tend to dominate the southern subtropical gyres, and cyclones the northern flank of the ACC. Major causes of regional polarity dominance are larger formation numbers and lifespans, with a contribution of differential propagation pathways of long-lived eddies. Areas of dominance of one polarity are generally congruent with the same polarity being longer-lived, bigger, of larger amplitude, and more intense. Eddies extend down to at least 2000 m. In the ACC, eddies show near surface temperature and salinity maxima, whereas eddies in the subtropical areas generally have deeper anomaly maxima, presumably inherited from their origin in the boundary currents. The temperature and salinity signatures of the average eddy suggest that their tracer anomalies are a result of both *trapping* in the eddy core and *stirring*.

1. Introduction

While the potential importance of eddies of lateral scales of a few tens to a few hundreds of kilometers was recognized early on [*Robinson*, 1983], the omnipresence of these features in the global ocean could only be truly acknowledged with the onset of satellite altimetry about two-and-a half decades ago [*Chelton et al.*, 2011b] (CSS11 thereafter). Eddies of these scales are typically referred to as "mesoscale." Mesoscale transient eddies, coherent vortices evolving at temporal scales of weeks to years and populating the world's oceans at any moment by thousands, likely contribute the major fraction to mesoscale kinetic energy (CSS11), which itself dominates the ocean's total kinetic energy [*Ferrari and Wunsch*, 2009]. This recognition, as well as the increasing availability of satellite observations and the ability to push the resolution of models down to the mesoscale, triggered extensive research on oceanic mesoscale features, such as fronts and eddies, and their impact on ocean circulation, climate, biogeochemistry, and ocean productivity [e.g., *McGillicuddy et al.*, 1998; *Jayne and Marotzke*, 2002; *Hallberg and Gnanadesikan*, 2006; *Beal et al.*, 2011; *Gruber et al.*, 2011; *Morrow and Le Traon*, 2012; *McWilliams*, 2008; *Treguier et al.*, 2014].

Eddy activity is particularly high in the Southern Ocean, a vast area with tremendous importance for global ocean dynamics [e.g., *Marshall and Speer*, 2012; *Talley*, 2013], the global uptake of anthropogenic carbon and heat [e.g., *Mikaloff Fletcher et al.*, 2006; *Frölicher et al.*, 2015], and low latitude productivity [*Sarmiento et al.*, 2004]. Eddies are formed here mainly due to instabilities of the dynamic Antarctic Circumpolar Current (ACC) and the boundary currents along the continents at the northern flank of the ACC. Southern Ocean eddies are not only numerous, they are also essential for ocean dynamics in the region as has been concluded by many studies [e.g., *Rintoul et al.*, 2001; *Naveira Garabato et al.*, 2004; *Fyfe and Saenko*, 2006; *Hallberg and Gnanadesikan*, 2006; *Mignone et al.*, 2006; *Hogg and Blundell*, 2006; *Zickfeld et al.*, 2007; *Lachkar et al.*, 2007; *Böning et al.*, 2008; *Hogg et al.*, 2008; *Thompson*, 2008; *Gillett et al.*, 2008; *Sallée et al.*, 2010; *Sallée and Rintoul*, 2011; *Morrison and Hogg*, 2012], yet many aspects of the impact of eddies and the underlying physical mechanisms remain unclear.

1.1. Southern Ocean Eddy Effects

Two major effects of eddies are commonly discussed: first, they balance the momentum input of the intensive westerly winds that blow over the Southern Ocean channel. The eddies achieve this balance by transporting the momentum by interfacial form stress downward toward the ocean bottom, where it is dissipated [*Johnson and Brydent*, 1989; *Nikurashin et al*., 2013]. Second, the eddies induce a meridional overturning circulation with associated transports of material properties, overcoming the barrier generated by the zonal flow of the ACC [*Abernathey et al*., 2010; *Naveira Garabato et al*., 2011]. In particular, this eddy-induced overturning causes a southward transport in the upper ocean that tends to offset the northward wind-induced Ekman transport [e.g., *Hallberg and Gnanadesikan*, 2006; *Ivchenko et al*., 2008; *Marshall and Radko*, 2003]. As the degree of cancellation depends, for example, on the vertical structure of these two respective transports [*Morrison and Hogg*, 2012], the resulting residual circulation may respond in rather complex manner to changes in atmospheric forcing in a changing climate. The extent of the compensation of the Ekman transport by eddies is essential, for instance, in the context of the hypothesized contemporary saturation of the Southern Ocean sink for atmospheric carbon dioxide [*Le Quéré et al*., 2007; *Lovenduski et al*., 2008]. Moreover, the eddy-induced upward transport of heat balancing the downward mean transport has gained attention more recently [*Zika et al*., 2013; *Morrison et al*., 2013; *Griffies et al*., 2015]. A third additional effect, which is generally not accounted for in models that do not resolve eddies explicitly, is the potential of coherent eddies to transport trapped water and its material properties quasi-isolated laterally over large distances, releasing it in a very different environment than where the eddy originated from. This effect can result in an upgradient tracer transport, in contrast to the eddy mixing effect, which is downgradient inherently. Finally, ocean eddies also alter atmospheric conditions, namely wind, cloud cover, and precipitation [*Frenger et al*., 2013; *Byrne et al*., 2015].

Ocean models used for climate change simulations often do not explicitly resolve eddies and rely on parameterizations of the eddy effects, the most commonly used being the *Gent-McWilliams parameterization* [*Gent et al*., 1995]. This scheme relies on the net effect of eddies being their tendency to flatten isopycnals, and thus parameterizes them as a downgradient diffusion of isopycnal thickness [see e.g., *Gent*, 2011, for discussion], resulting in an advective tracer flux. In addition, eddy mixing is typically parameterized by a scheme causing along-isopycnal tracer diffusion (*Redi diffusion*) [*Solomon*, 1971; *Redi*, 1982]. The associated eddy diffusion coefficients have been generally assumed to be constant or simply a function of some large-scale flow. In reality, the effects of eddies are more diverse and complex and are linked to the occurrence, characteristics, and life cycle of eddies, yet the relation between these eddy properties and their impacts on tracers and circulation remains incompletely understood, with few studies estimating eddy effects based on observable eddy properties (e.g., eddy tracer diffusivities based on eddy length scales and propagation speeds) [*Klocker and Abernathey*, 2014; *Bates et al*., 2014]. Thus, while new and extended parameterizations for the effect of eddies for noneddy resolving ocean models are needed, we are lacking a good description of the possible dependencies of the effects of eddies on the eddy properties, which in turn requires a thorough knowledge of the latter. Our goal here is to close this gap by determining and quantifying the properties of Southern Ocean eddies, providing the basis for the development of new parameterizations.

1.2. Focus of This Study

Our study builds on satellite observations of altimetry (resolution of 1/3°) and SST, which provide sufficient spatial and temporal coverage for conclusions on the large-scale and climatological distribution and properties of the larger mesoscale eddies. We combine these remote sensing products with the emerging temperature and salinity profile data from the Argo float array [*Roemmich et al*., 2009], permitting us to augment the surface-ocean-based analysis with a three-dimensional reconstruction of the eddy field. We employ a semi-Lagrangian approach, using the eddy center and lifetime as reference location and time, and using an automatied tracking algorithm to determine the eddy's life cycle. This approach will provide complementary information to the more frequently employed Eulerian framework. A similar approach was taken in several regional studies, e.g., for the Mediterranean [*Isern-Fontanet et al*., 2003, 2006], various areas in the Pacific [*Henson and Thomas*, 2008; *Chaigneau et al*., 2008; *Itoh and Yasuda*, 2010; *Kurczyn et al*., 2012; *Liu et al*., 2012], the eastern boundary upwelling systems [*Chaigneau et al*., 2009], Agulhas rings [e.g., *Dencausse et al*., 2010], and eddies in the Tasman Sea [*Everett et al*., 2012] (based on eddies detected by CSS11). This is the first such a study with a focus on the Southern Ocean.

We not only provide regional detail to the global study by CSS11 in terms of eddy characteristics but also extend their analyses substantially, namely by including an analysis of the spatial pattern of differences between

anticyclones and cyclones, by studying the effect of eddies on physical tracers (temperature and salinity) and by determining the subsurface structure of Southern Ocean eddies. Further, we add a more process-based discussion, highlighting three issues associated with eddies that may be of potential importance for the large-scale impact of eddies and hence parameterizations. These are (i) the spatial heterogeneity of eddies, especially the relation between eddies and topography, (ii) the differences between anticyclones and cyclones, i.e., the role of eddy polarity, and (iii) the potential of eddies to *stir* and *trap* tracers, i.e., local versus potential nonlocal effects of eddies. These three focal points are introduced in more detail in the following.

The high spatial heterogeneity of eddies is clearly evident in climatological maps of eddy kinetic energy, a combined measure for the frequency and intensity of eddies in a location. Even though eddies occur basically anywhere, they tend to be associated with Earth's major ocean currents, owing to baroclinic and barotropic instabilities favoring the generation of eddies [*Treguier et al*., 2007]. But even within these current systems and especially within the ACC, topographical obstacles cause particularly high eddy kinetic energy downstream [*Chelton et al*., 1990; *Sokolov and Rintoul*, 2009a; *Thompson et al*., 2010]. The close relations of eddies and topography itself have been noted previously [*Ansorge et al*., 2014], and *Fu* [2009] has commented on the connection of topography and eddy propagation patterns. We associate and further discuss in this paper topographical plateaus with noteworthy low levels of eddy activity in the Southern Ocean.

Our second focus, i.e., differences in eddy polarity, matters when considering eddy-induced tracer transport or the local effect of eddies on biology [*McGillicuddy et al*., 1998; *Siegel et al*., 2011] or the atmosphere [*Frenger et al*., 2013]. The reason is that anticyclones and cyclones show a similar anomaly but of opposite sign, i.e., anticyclones have a positive sea level anomaly, have elevated SSTs, and are characterized by thermocline downwelling, while the cyclones have a negative sea level anomaly, have lower than normal SSTs, and are characterized by thermocline upwelling (see schematic in Figure 1a). If the eddies of different polarities were to cooccur perfectly, the fact that anticyclones and cyclones generally show opposite anomalies would result in limited consequences, but the distribution of anticyclones and cyclones is asymmetric in space [*Griffa et al*., 2008; *Chaigneau et al*., 2009; *Saraceno and Provost*, 2012; *Chelton et al*., 2011b]. CSS11 noted, for example, that the formation of eddies due to symmetric pinching off from currents, such as the ACC, could lead to a cyclonic dominance equatorward of the front, and an anticyclonic dominance poleward of it. We examine polarity dominance for the Southern Ocean based on location of origin, death, characteristics, and evolution of eddies and discuss potential causes.

Finally, in order to estimate the impact of eddies on tracers, one needs to determine the extent to which eddies stir tracer gradients and the extent to which eddies trap water of certain tracer concentrations in their core and transport it to a distant place. *Stirring* is a local effect, that current model parameterizations aim to account for. *Trapping* [*Flierl*, 1981; *Chelton et al*., 2011b] is potentially nonlocal and not included in any of the existing parameterizations for coarse resolution models. Even though it appears that only few eddies trap perfectly [*Beron-Vera et al*., 2013], both modeling [*Donners and Drijfhout*, 2004; *Early et al*., 2011; *Nakano et al*., 2013] and observational based studies [*Lehahn et al*., 2011; *Ansorge et al*., 2009] indicate a significant degree of trapping by eddies. We argue for a superposition of both effects and on average not an insignificant contribution of *trapping* (over some distance, not necessarily over the complete eddy lifespan), based on the surface and subsurface pattern of temperature and salinity.

In the remainder of this paper, we will provide details about the data and methods we employed (section 2), present Southern Ocean eddy characteristics (section 3), discuss these results (section 4), and summarize and conclude in section 5.

2. Method

We use the same data and methods as in *Frenger et al*. [2013] to identify and track the eddies in the Southern Ocean, with few exceptions. The most important exception is that we augmented our data with colocated in situ measurements from Argo profiling floats in order to describe the depth structure of the ocean eddies. We provide here an extended description of the data and detection method, given the brevity of these descriptions in *Frenger et al*. [2013].

2.1. Data

The basis for the eddy detection is the sea level anomalies from Aviso from 1997 through 2010 between 30°S and 65°S (http://www.aviso.oceanobs.com, Delayed-Time v3.0.0, reprocessed March 2010). We chose to work

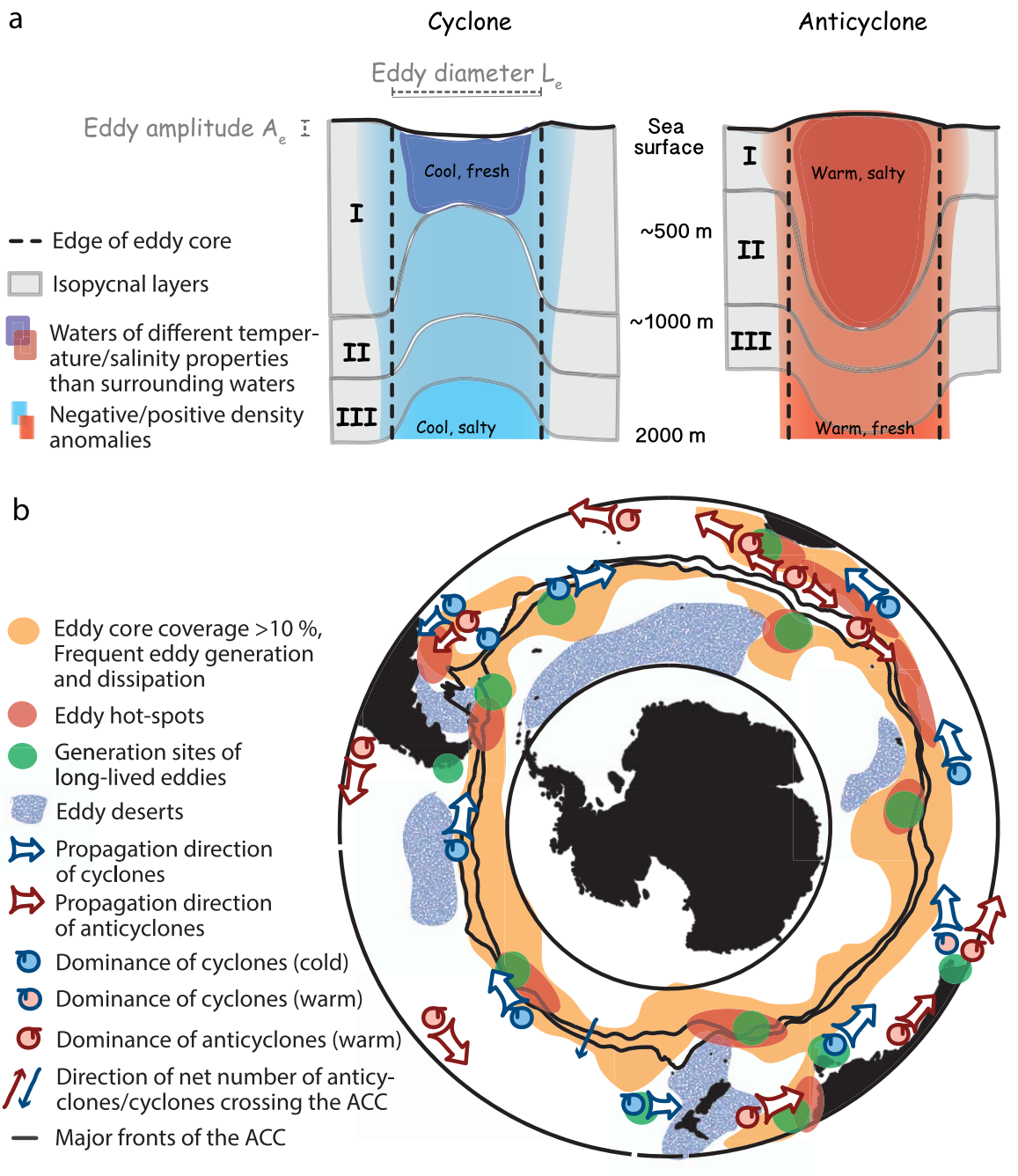

Figure 1. Summary of major findings with respect to Southern Ocean eddies. (a) Typical subsurface eddy structure, with three different regimes indicated: regime (I) where distinct temperature and salinity properties suggest trapping; regime (II) where the stratification (isopycnal layer thickness) in the eddy interior is clearly different compared to the environment; regime (III) where isopycnal layers in the eddy interior and eddy environment are very similar, and temperature and salinity anomalies associated with eddies likely can be explained largely by adiabatic heaving/lowering of isopycnals. (b) Spatial pattern of findings based on ocean surface data.

with sea level anomalies rather than absolute dynamic topography as the former represents a precursor of the latter, with the Aviso absolute dynamic topography calculated as the sum of sea level anomalies and an estimate of the *mean* absolute dynamic topography, as such containing additional sources of uncertainty, like an estimate of the geoid. Also, ocean mesoscale eddies represent deviations from the mean flow and hence are expected to be detectable more easily based on *anomalies* of sea level. Aviso sea level anomalies are a merged product, based on measurements of many altimetry missions, including Jason-1&2, Envisat, ERS-1&2, Topex/Poseidon, and GFO resulting in a significant improvement in the identification of mesoscale features [*Pascual et al.*, 2006]. The Aviso sea level anomaly data have a spatial resolution of 1/3° and a temporal resolution of 7 days,

which is sufficient for the detection of the larger mesoscale eddies and for their tracking over time. We linearly interpolated the sea level anomalies to 0.25° to match the SST data (see below). We did not high-pass filter the data prior to our analysis as the filter size is not objectively definable, filtering can cause an attenuation of mesoscale features (CSS11), and eddies are expected to be detected by the algorithm independent of large-scale sea level height anomalies due to thermosteric and halosteric effects.

We used the AVHRR Pathfinder SST for the tracking routine (version 5, http://www.nodc.noaa.gov, *Casey et al.* [2010], 4 km/daily, daytime measurements, linearly interpolated onto 0.25° and averaged to weekly, 1997–2009). To characterize the spatial pattern of temperature anomalies associated with the eddies (eddy composites), we obtained weekly estimates of SST from AMSR-E (microwave radiometer) with a spatial resolution of 0.25° from 2002 through 2009. The AMSR-E data are produced by Remote Sensing Systems (available at http://www.remss.com) and sponsored by the NASA Ocean Vector Winds Science Team as well as the NASA Earth Science MEaSUREs DISCOVER Project and the AMSR-E Science Team. From these data, we computed the SST anomalies by subtracting from each time step a monthly climatology we created from the weekly fields. AMSR-E SST have a later start data than AVHRR Pathfinder SST but the advantage of very few missing data, in contrast to roughly 50% of missing data due to cloud cover over Southern Ocean eddies in the AVHRR data.

To obtain information on the vertical structure of the Southern Ocean eddies, we downloaded temperature and salinity profile data from Argo floats from the Argo data base (http://www.Argo.ucsd.edu/Argo_data_and.html, data from 2001 through 2010) [*Roemmich et al.*, 2009]. We only analyzed data with a quality flag 1 (best) of the postprocessed ("adjusted") data and additionally excluded still existing outliers ($-2C^\circ > T > 30C^\circ$ or $33 > S > 37$, which roughly correspond to the lowermost and uppermost 0.02% of data points of salinity and 0.002% of temperature), included only data at pressures between 0 and 2000 dbar and with pressures monotonically increasing with depth, and discarded profiles containing only one data point. We also selected only those floats that surfaced in the vicinity of eddies in the same week an individual eddy had been detected in our analysis. We subtracted from these float profiles the Argo climatology developed by *Von Schuckmann et al.* [2009] available at http://apdrc.soest.hawaii.edu/projects/Argo, at the specific location and month of each float profile. We calculated potential density referenced to the surface based on the Thermodynamic Equation of Seawater – 2010 and used the associated Matlab routines provided at http://www.teos-10.org [*McDougall and Barker*, 2011].

To obtain the vertical structure of eddies, we binned the profiles (i) laterally according to distance from the eddy center, normalized by the individual eddy radius, into 0.25 bins up to a distance of three normalized eddy radii. Observations from the "eastern side" of an eddy (0°–180°) were assigned to the right side of the average eddy, and observations from the "western side" of an eddy (180°–360°) to the left side of the average eddy (see e.g., supporting information Figure S1). (ii) Vertically, we split up the data into 5 dbar pressure bins. The measurements in a certain bin (at a certain depth and distance from the eddy center) were averaged to get the value for the "average eddy." The value in the bin was set to missing if the number of measurements in the bin was smaller than three. The number of data points available in each bin is shown in supporting information Figure S1 for the three regions we are discussing in this paper. The general results were insensitive to reducing the sample size by half in a random selection (not shown).

For the positions of the main ACC fronts (Polar Front and Subantarctic Front), we used geographical analyses by *Sallée et al.* [2008] (http://ctoh.legos.obs-mip.fr, 1997–2010). Further, we used an ocean dynamic topography as representation of the long-term mean geostrophic flow in the area (1992–2002 mean, from http://apdrc.soest.hawaii.edu/projects/DOT) [*Maximenko et al.*, 2009].

Finally, we needed an ocean current climatology for the tracking of eddies, which we derived from the ocean reanalysis SODA (0.5°/monthly, http://dsrs.atmos.umd.edu, *Carton and Giese* [2008], version 2.0.2, 1958–2001), and additionally information about the inherent propagation speed of eddies (from http://www-po.coas.oregonstate.edu/research/po/research/rossby_radius) [*Chelton et al.*, 1998], which is similar to the ones of long baroclinic Rossby waves.

2.2. Mesoscale Eddy Detection

2.2.1. Eddy Identification

We identified the mesoscale eddy instances using the Okubo-Weiss parameter (OW) [*Okubo*, 1970; *Weiss*, 1991], which has been extensively used for this purpose [e.g., *Isern-Fontanet et al.*, 2003; *Chelton et al.*, 2007; *Chaigneau et al.*, 2008; *Henson and Thomas*, 2008; *Itoh and Yasuda*, 2010].

The OW parameter measures the dominance of vorticity over strain at a particular location,

$$\mathrm{OW}=s_n^2+s_s^2-\omega^2, \quad (1)$$

where $s_n=u_x-v_y$ is the normal and $s_s=v_x+u_y$ the shear component of the strain, and where $\omega=v_x-u_y$ is the relative vorticity, with the subscripts denoting the partial derivatives in eastward and northward direction, respectively. The variables u and v in equation (1) are the eastward and northward surface current velocity anomalies, respectively, which we estimated from sea level anomalies through geostrophy.

Negative values of OW denote areas where vorticity is dominant, i.e., where an eddy might be present. We separated anticyclonic (anticyclones) and cyclonic (cyclones) eddies by the sign of their vorticity (anticyclones: positive and cyclones: negative), which ensured that features that consist of two neighboring eddies of both polarities are split. Further, we required the existence of a local minimum (cyclones) or maximum (anticyclones) of sea level anomalies within the eddy area.

For the calculation of the OW parameter with equation (1), we used the Aviso data on the original grid. The eddies were identified using $\mathrm{OW} < -0.2\sigma_{\mathrm{OW}}$ [*Pasquero et al*., 2001], where σ_{OW} denotes the spatial standard deviation of the OW. This standard deviation was calculated for each time step over the whole analysis domain and then averaged over time. Grid boxes with detected eddies were assigned a value of 1, while all other boxes were assigned a 0, and the resulting map with the detected eddies interpolated to a 0.25° grid.

We define the center of the eddy as its center of mass. Following many previous studies, we determine the diameter L_e of the eddies as the diameter of a circle covering the same area as the respective eddy

$$L_e=2\sqrt{A/\pi},$$

with the area A calculated as the sum of the area of the grid boxes an eddy is occupying. We calculated the eddy amplitude A_e as the absolute difference between the local sea level anomaly extremum of the eddy and the mean sea level anomalies over the eddy's edge. Here the eddy edge is defined as a ring with a width of one grid box (0.25°) around the eddy core. The eddy intensity ζ is defined as the sea level anomaly gradient related to the eddy, i.e., eddy amplitude over radius

$$\zeta=A_e/(L_e/2).$$

This is a better proxy for the dynamic intensity of an eddy than either L_e or A by themselves as it is related to the swirl velocity, which in turn is frequently employed in combination with the eddy propagation speed to assess the eddy "nonlinearity" [*Flierl*, 1981; *Chelton et al*., 2007]. As a simple measure for the integrated eddy energy, we use the eddy kinetic energy summed over the eddy area, where the eddy kinetic energy was calculated for each grid box based on the same geostrophic velocity anomalies used in equation (1). Another expression we use is "eddy impact area" motivated by the fact that a tracer is clearly impacted beyond the OW eddy core: based on the eddy composites, we defined the eddy impact area as a circle of 3 times the eddy radius see section 2 and 3.4 and associated Figures.

To resolve the horizontal structure of the mean eddy as detected at the ocean surface, we extracted individual squared subregions for each identified eddy from the weekly maps of sea level anomalies and SST. The size of the extracted squares was five diameters (10 radii) containing the core of the eddy at the center. This is a large enough area to include the eddy's impact on its surroundings. Defining the squares side lengths in terms of the individual eddy radii implied an implicit standardization. Finally, we produced a mean spatial map by averaging over all eddies (eddy composite). The results were insensitive to rotating the eddies according to the large-scale SST front as the SST gradient is oriented north-south to first order. We attribute the variance of the SST anomaly (V_{total}) associated with eddies

$$V_{\mathrm{total}}=\sum_{i=1}^{n}\left[\Delta\mathrm{SST}(\mathrm{total})_i\right]^2, \quad (2)$$

to a contribution of a monopole versus a dipole pattern of the total SST anomaly (see section 4.4). Here ΔSST is the eddy composite SST anomaly and n the number of pixels of the eddy composite within a radius of three eddy radii of the eddy center (see section 3.4 and associated Figures). Then, we calculate the variance explained by the monopole contribution of the SST anomaly as $V_{\mathrm{monopole}}/V_{\mathrm{total}}$, where V_{monopole} is

calculated as in equation (2) but with ΔSST(total) being replaced by the monopole SST anomaly. The calculation for the variance explained by the dipole is analogous.

Eddy properties are mapped back into space by binning into longitude-latitude bins of various sizes, with the size chosen depending on the number of available data points. A relatively large sample size is available when using weekly snapshots of eddies. Weekly snapshots are used for instance for the calculation of mean eddy diameters and amplitudes. In contrast, a relatively small sample size is available for once-per-lifetime-properties of eddies, such as lifespan or distance covered over the complete lifespan. In the latter case, bin sizes are substantially larger to reduce noise. The minimum number of data points per bin is set to five for calculating the ratio of properties of anticyclones over cyclones. To assess if property distributions of anticyclones and cyclones are different, the Kolmogorov-Smirnov significance test is applied [*Massey*, 1951].

For many of the analyses, we separate the eddies into a northern and southern group with the separation being determined by the long-term mean position of the −20 cm sea surface height contour (see supporting information Figure S3). We chose this level based on maps of eddy tracks which we derived. The contour largely separates eddies north of the ACC propagating westward and eddies propagating eastward because they are being impacted by the ACC.

2.2.2. Eddy Tracking

The tracking of mesoscale eddies is more error-prone than their detection [see e.g., *Neu et al*., 2013]. Dynamic areas such as the ACC are especially challenging, as the eddies tend to follow somewhat "chaotic" paths [*Petersen et al*., 2013]. We tested various parameters and additions to our algorithm based on a visual evaluation before we found satisfying results. The tracking method is explained in full length in *Frenger et al*. [2013, supporting information].

To decide if for an eddy in the current time step a matching eddy existed in the subsequent time step, we took into account several factors: first, the distance the eddy was expected to be displaced in the time period of a week corresponding to the temporal resolution of the data we used. The movement is affected by the eddy intrinsic propagation speed and advection by the ambient current. To account for these effects, the displacement was estimated as the sum of the propagation by linear baroclinic Rossby waves [*Chelton et al*., 1998] and by the barotropic part of the SODA mean current. We searched for a potential match around this projected location within a search ellipse, determined on the basis of the zonal and meridional variability of the mean currents (semiaxes of σ_u and $3\sigma_v$, with u and v representing the SODA mean current velocity components). We set one L_e as the minimum length for the semiaxes to allow for additional effects as well as uncertainties, such as deviations of the eddies' phase speeds from the ones of baroclinic Rossby waves and the small poleward and equatorward deflection of cyclones and anticyclones, respectively [*Cushman-Roisin et al*., 1989; *Morrow*, 2004; *Van Leeuwen*, 2007], as well as for eddy-eddy interactions [*Chelton et al*., 2011b; *Early et al*., 2011].

Then, we applied a similarity criteria to constrain matchups to eddies of roughly similar properties [*Penven et al*., 2005]. If more than one eddy snapshot e_i was found within the search ellipse for eddy e_0, we calculated a dissimilarity measure $D_{e_0}(e_i)$ for each of the possible snapshots e_i

$$D_{e_0}(e_i)=\sqrt{\frac{1}{4}\left[\left[\frac{\Delta\omega}{\sigma_\omega}\right]^2+\left[\frac{\Delta A}{\sigma_A}\right]^2+\left[\frac{\Delta T}{\sigma_T}\right]^2+\left[\frac{\Delta d}{d_\mathrm{m}}\right]^2\right]},$$

and selected the snapshot with the smallest $D_{e_0}(\mathrm{e}_i)$. Here $\Delta\omega=\omega_{e_0}-\omega_{e_i}$, $\Delta T=T_{e_0}-T_{e_i}$, $\Delta A=A_{e_0}-A_{e_i}$, $\Delta d=p_0-x(\mathrm{e}_i)$, and d_m is the smallest distance between e_0 and any e_i, i.e., the minimum of Δd. p_0 is the estimated new position of the eddy, $x(\mathrm{e}_i)$ the location of snapshot e_i, and ω, A, and T are the relative vorticity, amplitude, and surface temperature of the eddy core, respectively. σ denotes the temporal standard deviation of the respective property at the eddy location.

The new snapshot had to fulfill two criteria: first, the dissimilarity $D_{\mathrm{e}_0}(\mathrm{e}_i)$ had to be smaller than one to exclude highly unlikely changes in eddy properties. Second, to filter out dying eddies, the eddy vorticity was not allowed to increase by more than 5% if the vorticity had decreased during the last three time steps and was less than half of the eddy's original vorticity. An eddy was assumed to have died if no suitable snapshot was found. We did not try to recover any lost eddy in subsequent time steps.

The merging and splitting of eddies pose a major difficulty for any automated tracking algorithm. We cannot quantify and therefore did not attempt to account for these processes. Given our criteria, we treated

the merging of two eddies, for example, as the continuation of one—the more similar—eddy, and the death of the other eddy. Eddy "birth" and "death" are defined as the time of first and last detection of a trackable feature and refer to the emergence and disappearance of an eddy of certain characteristics. If the eddy changes its characteristics abruptly, such as through merging or splitting, the eddy of these characteristics has "died" in our definition. Similarly, an eddy may "die" if it decreases its size in the end of its lifetime until it falls below the detection limit. For this reason, we avoided the term "dissipation." We excluded eddies from our analysis with birth or death times outside our analysis period to consider only eddies with complete life tracks.

As we track eddies only in the Southern Ocean, eddies may propagate in and out of the domain across the northern or southern boundaries (30°S and 65°S, respectively). We did not exclude these eddies from our analysis but this must be kept in mind for figures of eddy properties that depend on lifespan, such as the lifespan itself or propagation distances.

2.3. Uncertainties and Limitations Due to Data Resolution

We introduced a few constraints to reduce noise in the detected and tracked eddies. First, we required eddies to feature a local sea level anomaly extremum. Second, we rejected features with a maximum width of only a single grid box (0.25°) in order to avoid the identification of elongated features as eddies. Third, we required four adjacent grid boxes as the minimum to form an eddy. Our constraint on the minimum size of eddies is at the very limit of what is resolved by the altimetry data. Finally, we required eddies to appear in at least four consecutive time steps, i.e., over at least 4 weeks. Even though many of the shorter-lived features may be significant, the constraint of a lifespan of 4 weeks is advisable due to the preprocessing of the Aviso data, which involves spatiotemporal filtering (CSS11).

The OW parameter method to detect eddies has been criticized and a number of alternative methods have been proposed. For example, it was pointed out (i) that the OW method only identifies the pure core of the eddy, and thus underestimates the total eddy area, (ii) that it tends to overdetect eddies, (iii) that it is very sensitive to noise amplification because of the involvement of double derivatives [*Chaigneau et al*., 2008; *D'Ovidio et al*., 2009; *Chelton et al*., 2011b], and (iv) that it involves a threshold which needs to be chosen. The first point represents no flaw of the OW parameter but needs to be kept in mind when comparing the eddy diameters of this data set to eddy data sets where a geometric criterion was used, such as the outermost closed sea level anomaly contour. The second and third points introduce noise, which we reduced by filtering the eddies with a constraint on the lifespan (4 weeks, see previous paragraph). The large number of identified eddies also helps to keep the results significant. We chose the OW method, because it is well tested for ocean applications and computationally efficient. The fourth point, i.e., the threshold, is an issue that the OW method shares with other standard detection methods. The use of the spatial mean of the standard deviation of the OW as the threshold in combination with the large spatial variability of sea level variance in the Southern Ocean potentially implies an implicit focus on intense eddies.

As commented on previously, due to the limitations of the resolution capability of the sea level anomaly data, we discuss here the larger mesoscale eddies, leaving aside smaller-scale mesoscale and submesoscale coherent vortices. As a crude estimate, a feature of 3 times 3 grid boxes can be resolved, which corresponds to slightly less than 50 and 100 km at 65°S and 30°S, respectively. This estimate roughly agrees with the estimate of the resolution capability of an earlier Aviso version by CSS11 based on spectral analysis. It is also supported by a dropoff of eddy numbers of diameters of 50 km and less at 65°S, and of 80–100 km at 30°S (supporting information Figure S2).

We note that we discuss only eddies which are detectable at the surface based on sea level anomalies, i.e., we neglect eddies in the ocean interior which are known to exist, also in the Southern Ocean [*Arhan et al*., 2002]. However, *Petersen et al*. [2013] found based on an extensive three-dimensional eddy detection in a high-resolution global ocean model that only a few percent of eddies are subsurface and concluded that sea surface data provide a good tool to investigate ocean eddies.

3. Results

We identified nearly one million single eddy instances in the Southern Ocean (south of 30°S and north of 65°) in the weekly data over the analyzed time period 1997–2010, constraint by the resolution capability of

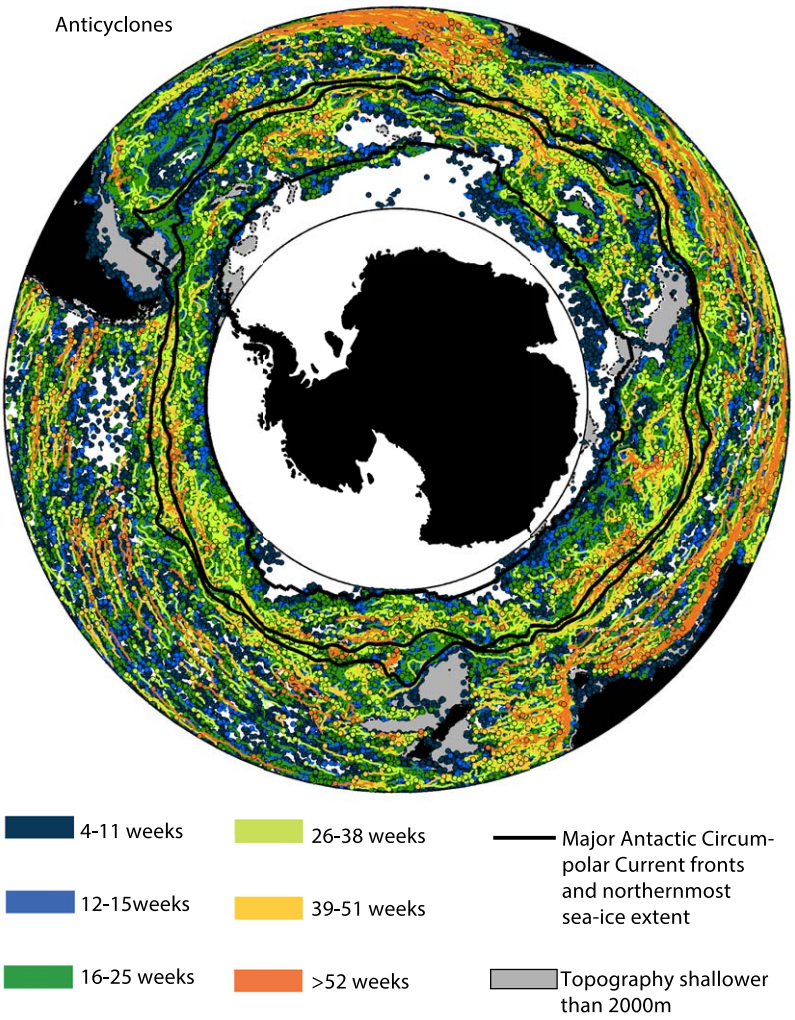

Figure 2. Overview of eddy data set as compiled and analyzed in this paper: dots mark initial positions of eddies (birth locations) and lines the propagation paths (tracks), colored by age; anticyclones detected and tracked over the time period 1997–2009 between 30°S and 65°S; eddies with longer lifespans are plotted on top of the eddies with shorter ones; note that lifespans of eddies propagating into or out of the domain are underestimated; black lines show from north to south the mean northern (Subantarctic Front) and southern (Polar Front) positions of the Antarctic Circumpolar Current fronts (based on *Sallée et al.* [2008]), and the northernmost extent of missing sea level anomaly data due to sea-ice; gray shaded areas mark topography shallower 2000 m; only eddies with a minimum lifetime of 1 month are considered (this applies to all subsequent figures).

Aviso to minimum diameters of approximately 50 km at 65° and 100 km at 30°, all fulfilling our detection criteria that they belonged to eddies that were detected at least 4 times, i.e., over a month. The one million individual eddy instances resulted in approximately 10^5 tracked eddies existing 4 weeks or longer. The frequency of eddies decreases steeply with longer lifespans (see below). We observed less than 1% to live longer than 1 year, and several tens of eddies (10 anticyclones and 41 cyclones) lived longer than 2 years. These extremely long-lived eddies were almost exclusively found north of the ACC.

The propagation paths of all eddies tracked over at least 1 month in Figures 2 and 3 reveal details about the eddies in the Southern Ocean. The figures visualize where eddies occur preferably (in the vicinity of strong currents), where they propagate to over their lifetimes (strongly affected by large-scale advection and topography, see also Figures 4 and 5), how old eddies get (weeks to years), where we find the long-lived eddies (undisturbed subtropical regions and the regions of high sea level variability associated with the ACC, especially for cyclones), where eddies are generated (strong currents and in association with topographical features, see also Figure 4) and dissipate (also within strong currents, further west from their location of origin in the southern subtropical gyres), and how anticyclones and cyclones differ in all these

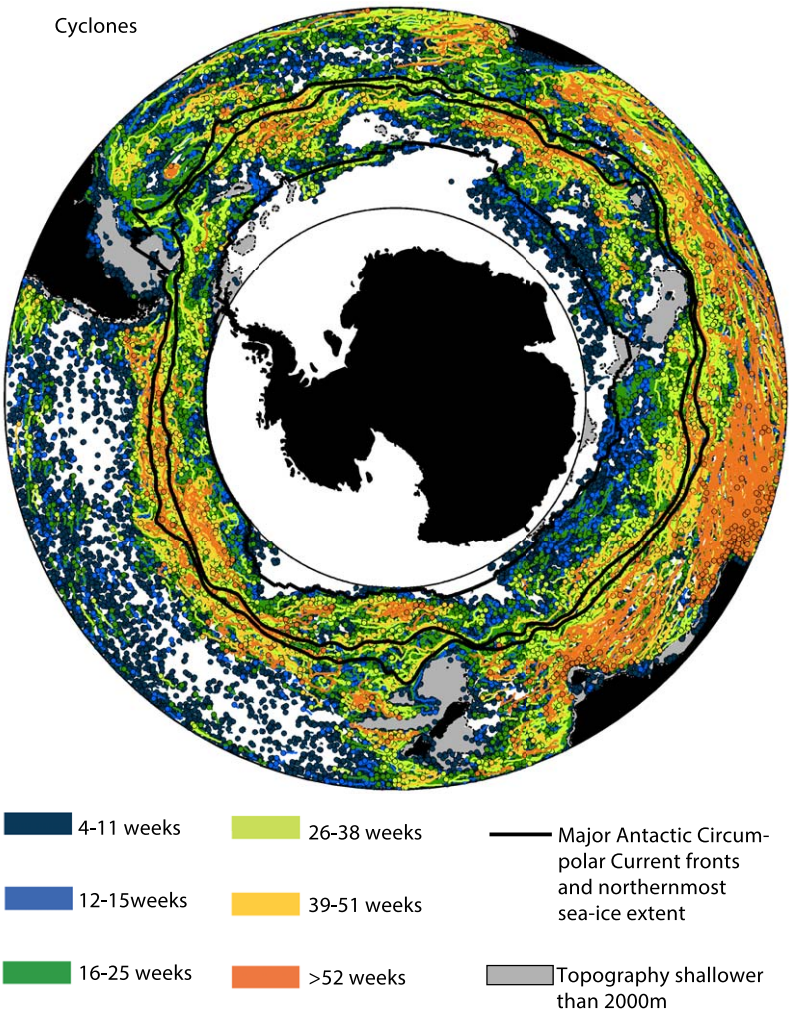

Figure 3. Same as Figure 2 but for cyclones.

aspects (e.g., many more anticyclones than cyclones populate the south Pacific, and anticyclones and cyclones propagate in undisturbed waters steadily equatorward and poleward, respectively). We discuss each of these aspects in sequence next.

3.1. Eddy Distribution

The Southern Ocean in most parts is truly rich in mesoscale eddies. The dynamic regions of the Southern Ocean, i.e., regions of intense mean currents and large sea level height variability are covered with the cores of mesoscale eddies that exist at least 1 month more than 25% of the time (Figure 6a). The coverage in hotspot regions rises to more than 50% and to more than 75% if one considers an eddy impact area of two or three eddy radii, respectively (see sections 2 and 3.4). But there are also regions where very few or literally no eddies occur. A largely zonal picture emerges to first order, with weak eddy activity in the northern part of the domain, i.e., at subtropical latitudes, and strong activity along the ACC. Zonal variability is superimposed on this pattern with eddy-rich waters near continents and very low eddy activity in the subtropical gyres in the north of the domain. Furthermore, the Pacific shows a lower eddy coverage than the Atlantic and Indian Ocean in the subtropical gyres. The ACC pathway also shows variation in its eddy activity with higher activity downstream of topographical features (apparent also in the global map of eddy centroids of *Faghmous et al*. [2012], but not clearly visible in CSS11).

Areas of high eddy occurrence are associated with strong currents, such as the ACC and the western boundary currents, as well as the regions where they interact, such as the confluence zone of the Brazil and

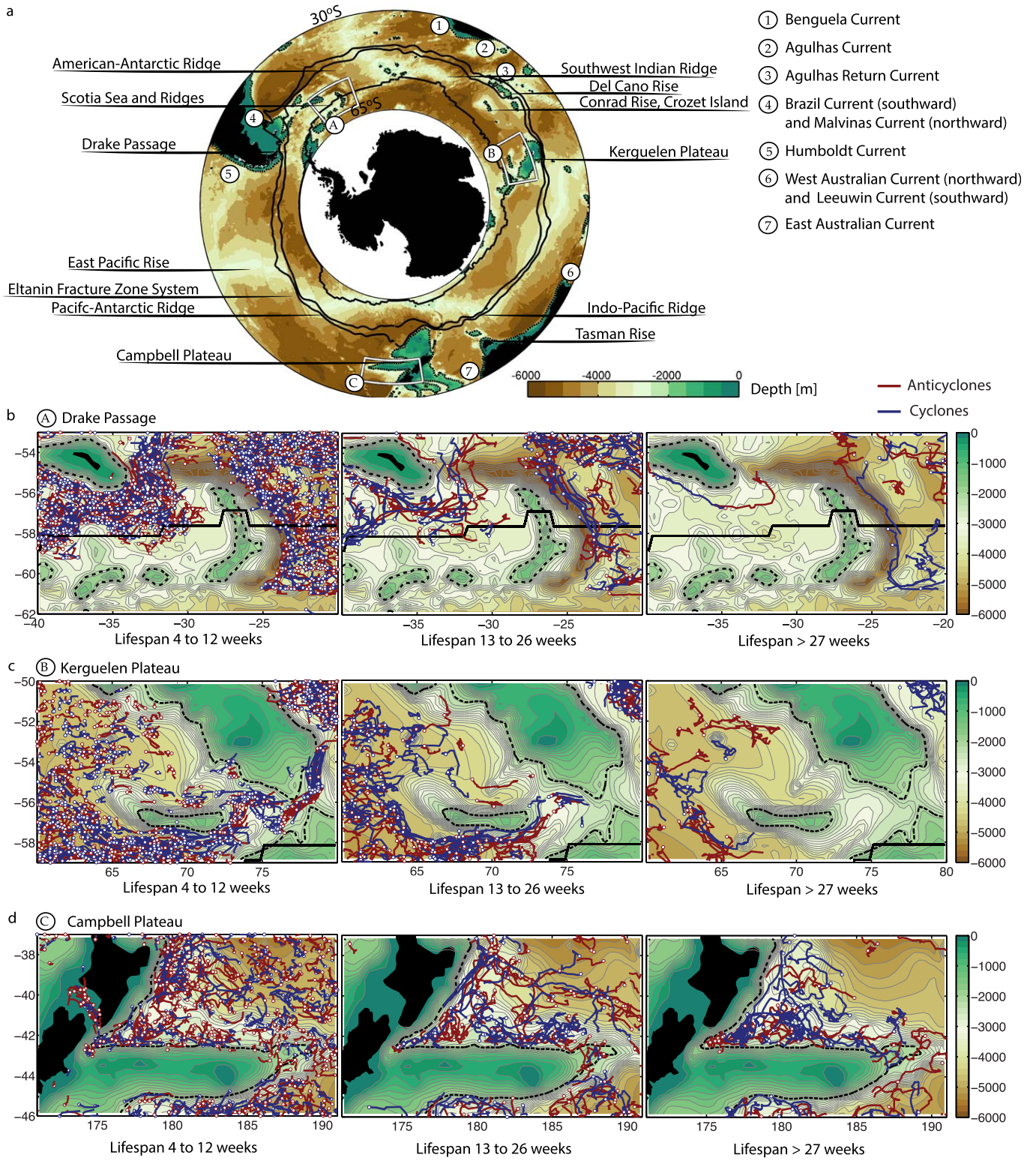

Figure 4. Eddy propagation pathways and topography: zoom-in on tracks of eddies at selected topographical features. (a) Southern Ocean topography with labeling of selected topographical features; white squares denote the zoom-in regions as shown in Figures 4b–4d, namely an area around the Drake Passage, around the Kerguelen Plateau and around the Campbell Plateau; distinguished by anticyclones (red) and cyclones (blue), and three age groups with short-lived eddies shown in the left column and longer-lived eddies in the middle and right columns; the location of first detection is marked with a white circle for each individual eddy; as in Figure 2, black lines show from north to south the mean northern and southern positions of the ACC major fronts, and the northernmost extent of sea-ice related missing sea level anomaly data; dashed black contours show the −2000 m topographical isoline.

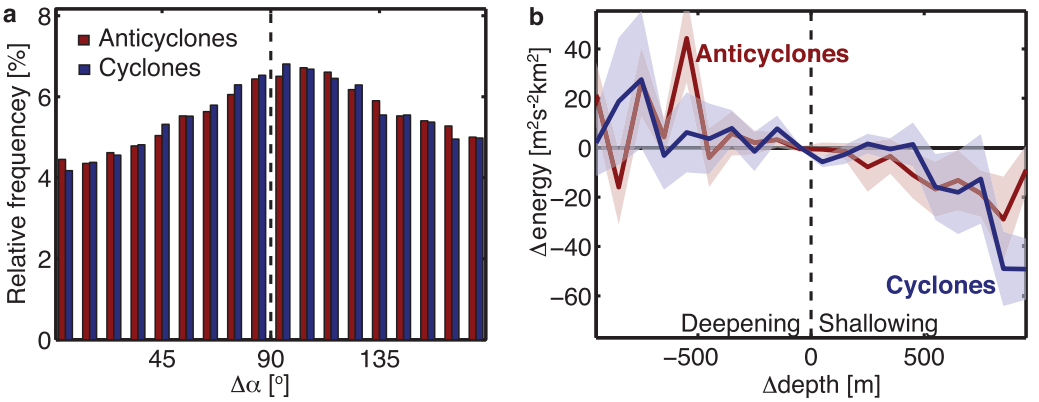

Figure 5. Relationship of eddies and topography. (a) Angle α between propagation direction of eddies and topographical gradient ($0^\circ < \alpha < 90^\circ$ implies a propagation into shallower waters); based on 10° bins; (b) water depth difference at the location of the eddy relative to the depth at the preceding lifetime step of the eddy, and associated change in eddy kinetic energy integrated over the eddy area; based on 100 m bins, shading shows the standard error of the mean; only eddies are included which occurred in water of 3000 m and shallower.

Malvinas Currents at about 40°S east of South America and the Agulhas Retroflection and Agulhas Return Current (Figures 2, 3, and 6a; refer to Figure 4a for current and topographical labeling). In contrast, the eastern boundary currents (to the extent they are included in our domain) show relatively weak eddy activity, although with distinct differences. The Humboldt Current off the South American coast emerges as the eastern boundary current system with the least eddy activity, while the Benguela and Leeuwin/West Australian Current Systems tend to have more eddies. Looking at the ACC eddy band, it is noteworthy that the largest eddy occurrence is located just south of the Polar Front (see also supporting information Figure S3). The eddy coverage drops off quite abruptly at the ACC's northern flank but levels off more gradually to the south.

Most interestingly, there are also distinct eddy-free areas. The most prominent ones of these eddy deserts [*Henson and Thomas*, 2008] are the regions of relatively shallow topography, i.e., plateaus with water depths of less than 2000–3000 m where the Rossby deformation radius is very small (e.g., shown in gray in Figure 6a, also apparent in CSS11 [their Figure 5] and *Faghmous et al*. [2012, Figure 6]), such as the Kerguelen Plateau, the Campbell Plateau, and the Conrad/Del Cano Rise/Crozet Island. This finding does not depend critically on the criteria we used to identify and track eddies. If we chose to include short-lived (<1 month) eddies, the coverage by eddies over shallow topography increases only to a limited extent (not shown).

Another area of almost nonexistent eddy activity occurs south of the northernmost extent of sea-ice (Figures 6a, 2, and 3). However, we consider this finding as not particularly robust, since satellite altimetric measurements could be biased close to sea-ice and cannot measure sea level beneath sea-ice at all. Although surface drifters find this region to be similarly low in eddy coverage, this method is also seriously affected by the presence of sea-ice. Nevertheless, it is intriguing to consider that eddy activity might be reduced in areas of seasonal sea-ice cover.

Eddy occurrence varies much less in time than in space. While eddy occurrence varies seasonally and on longer term only by about 10%, the eddy occurrence varies by more than 100% between the subtropical waters and the ACC (supporting information Figure S3, see also *Chaigneau et al*. [2009]).

3.2. Eddy Propagation and Death

The majority of the eddies do not propagate far from where they formed. Even though eddies may live long, propagate, and get advected, they are mostly restricted to propagation distances of *O*(10–100) km over their average lifetime (Figure 7b, see also modeling study by *Petersen et al*. [2013]). One reason for these relatively short propagation distances is that the intrinsic phase speed of eddies is relatively low, especially at high latitudes. Furthermore, the intrinsic eddy propagation direction (westward) and the eastward zonal advection by the large-scale circulation (ACC) work in opposing directions. Eddies cover smaller mean distances (*O*(10) km) in the South Pacific and South Atlantic than in the Indian Ocean and the vicinity of the ACC (*O*(100) km). Some differences between anticyclones and cyclones exist, with cyclonic eddies translating shorter distances in the South Pacific and Atlantic but longer ones in the Indian Ocean and in the vicinity

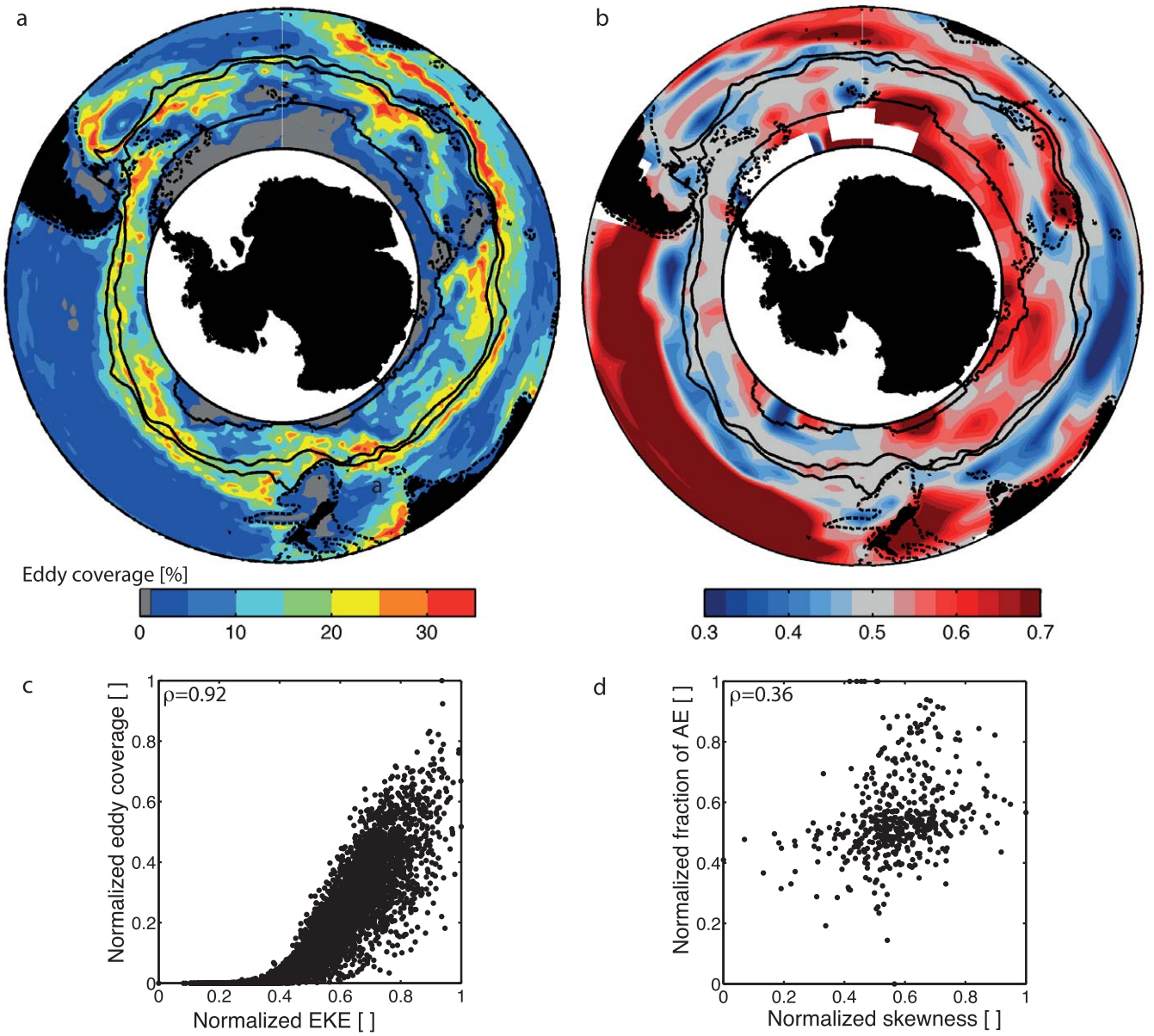

Figure 6. Area coverage by eddy cores and polarity dominance. (a) Averaged coverage by eddy cores over time (based on a 2° × 1° grid, linearly interpolated). (b) Ratio of area occupied by anticyclones (AE) over area covered by all eddies, thus values >0.5 in red and <0.5 in blue mark dominance of anticyclones and cyclones, respectively (based on a 8° × 3° grid, linearly interpolated); as before, solid black lines show the mean northern and southern boundaries (major fronts) of the ACC, and the southernmost contour of the northernmost extent of missing values due to sea-ice; dashed black lines mark the −2000 m depth contour. (c) Scatterplot of area coverage (as in Figure 6a) and the natural logarithm of eddy kinetic energy, and (d) scatterplot of polarity dominance (as in Figure 6b) and the skewness of sea level anomalies; ρ in the upper left corner indicates the Spearman correlation coefficient.

of the ACC when compared to anticyclones. Overall, even if eddies propagate around 1000 km, which the long-lived eddies in the subtropics do (less than 1% of the eddies, see first paragraph of section 3), the majority of these eddies stay in the same ocean basin (see also eddy tracks in Figures 2 and 3).

The fact that eddies on average do not propagate over vast distances is evident also by the similarity of the spatial pattern of eddy nurseries and graveyards (supporting information Figures S4a, S5a, and S5b). Especially in the dynamic regions of the ACC, the bulk of eddies emerges and disappears in the same dynamic regions downstream of shallow topography and, interestingly, south of the major fronts of the ACC.

The close relationship of eddy propagation paths and topography is obvious from a regional zoom on the eddy distribution figure, Figure 4b, which shows that (i) eddies generally do not occur over topographical

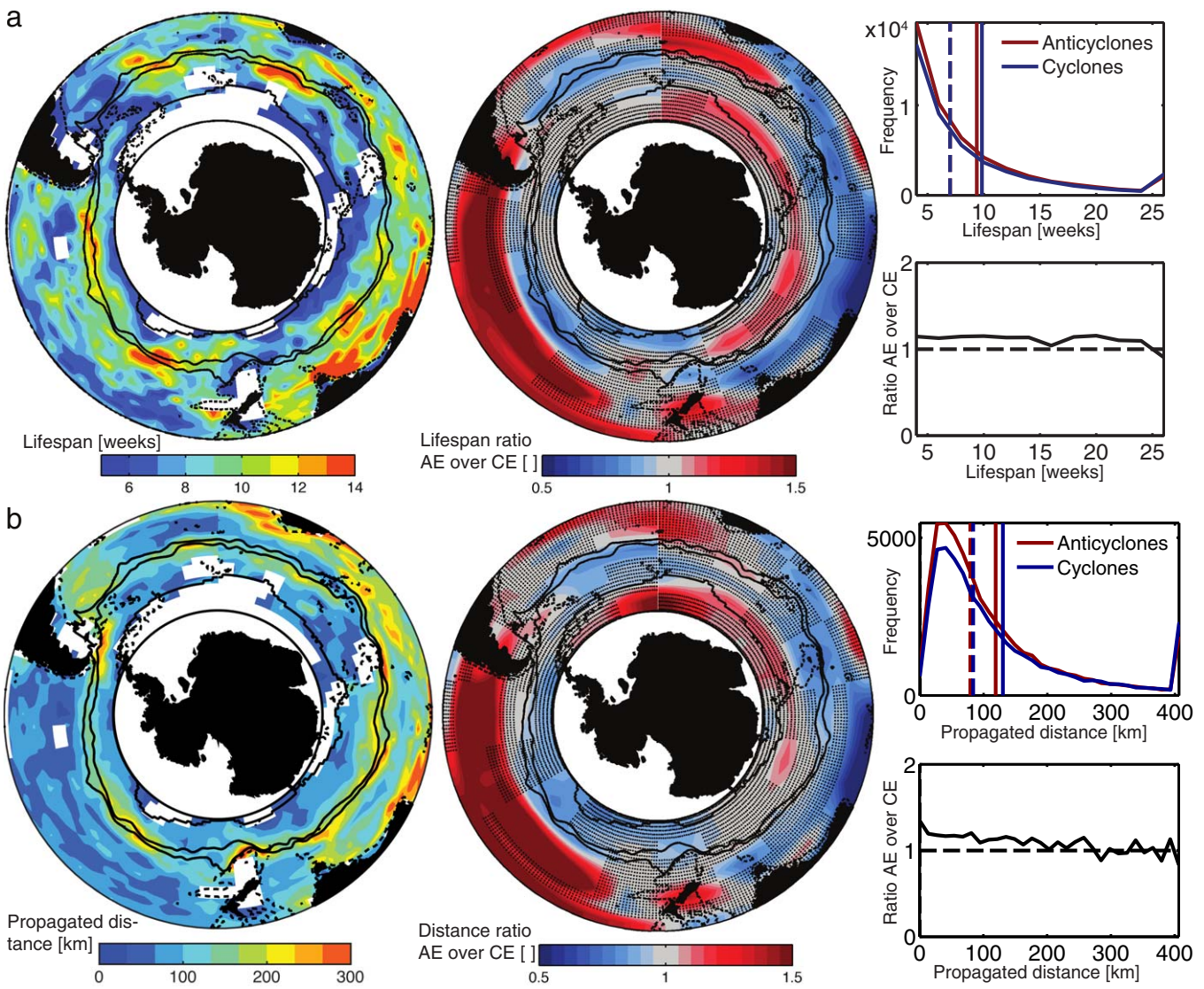

Figure 7. (a) Eddy lifespans and (b) propagation distances; (left) mean over all eddies (based on a 4° × 2° grid, linearly interpolated); (middle) ratio of the respective property for anticyclones (AE) over cyclones (CE); stippling marks boxes where the property distributions of cyclones and anticyclones are not significantly different (Kolmogorov-Smirnov test, $p = 0.05$, based on a 20° × 5° grid, linearly interpolated); main fronts and northernmost sea-ice extent are shown again as black solid contours, and topography shallower than 2000 m as dashed contour; (right column) property distributions distinguished by anticyclones and cyclones and ratio of distributions; eddy numbers are binned into 30 equally spaced bins; the final 31st bin at the upper end of the horizontal axis accumulates all eddies of the right tail of the distribution outside the range of the horizontal axis; vertical lines mark the mean (solid) and median (dashed).

features shallower 2000 m along the ACC and (ii) that longer-lived eddies tend to stay in even deeper waters than eddies of shorter lifespans (compare age groups in Figure 4b, i.e., the left column relative to the right column). The close relationship of eddies and topography is also supported by the lack of eddies crossing contours of topography in the first place (Figure 5a), and by eddies becoming both smaller and weaker in amplitude when propagating onto shallower topography resulting in a weakening of integrated eddy kinetic energy (Figure 5b).

The major propagation direction of eddies is westward (supporting information Figure S6a), as expected (CSS11). The main exception is the eddies in the ACC influence area, where most eddies propagate eastward, driven by the strong mean current of the ACC. The intrinsic meridional propagation of the eddies is equatorward for the long-lived anticyclones and poleward for the cyclones [*Cushman-Roisin and Beckers*, 2011; CSS11]. However, the intrinsic meridional propagation speed tends to be small, which results in a relatively incoherent or even "chaotic" spatial pattern especially in the influence regions of the ACC [*Petersen*

et al., 2013] owing to the strong overcompensation by the background meridional deflections of the mean current (supporting information Figures S6b and S6c). Nevertheless, the majority of the cold-core, negative sea level anomaly, cyclones tend to traverse the ACC from south to north (roughly 30 eddies per year on average). In the ACC, the intrinsic meridional propagation of eddies tends to lead to eddies merging back with the current they pinched off from, i.e., in the case of anticyclones, while typically being pinched off toward the south, they subsequently propagate northward toward the current they pinched off from.

3.3. Eddy Characteristics

Within our analysis domain, the mean eddy with a lifespan of at least 1 month has a core diameter of 85 (80) km, an amplitude of 12 (8) cm, a propagation speed of 0.04 (0.03) m s^{-1} (i.e., 22 (17) km $week^{-1}$), lateral turnover times of 24 (23) days, a lifespan of 10 (7) weeks, and propagation distances over their entire lifetime of 124 (81) km, with the bracket values denoting the median (see also Figures 7 and 8, right columns). The mean life cycle of an eddy consists of a spin-up and a spin-down phase lasting each 20% of its lifetime and a roughly steady phase in between (supporting information Figure S7, see also *Liu et al*. [2012], *Frenger* [2013], and *Samelson et al*. [2014]). Figure 2 and 3 can be translated into maps of long-term mean eddy properties, for instance of mean diameters and amplitudes of eddies (Figures 7 and 8, left columns). In general the large amplitude, large and intense eddies cluster along the major currents. The feature of large eddies occurring in association with major currents partly overwhelms the pattern of decreasing diameters with higher latitudes associated with the deformation radius (not shown). Eddies of highest integrated energy (a result of a combination of amplitude and eddy diameter, see section 2) are clearly western boundary current eddies, followed by ACC hot-spot eddies (not shown).

Slightly more of the analyzed eddies are anticyclonic than cyclonic, i.e., 52,092 (52.9%) anticyclones versus 46,312 (47.1%) cyclones. However, the distribution of polarity is reversed for long-lived eddies relative to the shorter-lived ones (see also Figure 7a right column). Of the very long-lived eddies (more than 1 year old), 60% are cyclones and 40% anticyclones. The maximum lifetime of eddies we were able to identify was 185 weeks for anticyclones and 166 weeks for cyclones, more than 3 years for both polarities.

There are also strong differences in the spatial distribution of the dominance of one polarity of eddies over the other, with one of the two polarities contributing up to 80% to the eddy coverage in a few areas (Figure 6b). The pattern is zonal to first order, with more anticyclones occurring south of the ACC and in the subtropical regions. In contrast, we find more cyclones in the ACC region and especially at its northern flank. The zonal band of cyclonic dominance at the northern flank of the ACC is broader in the Indian Ocean and is interrupted south of Africa, likely due to the extensive and intense Agulhas Current System.

Not only the spatial coverage of anticyclones and cyclones differs but also their properties (Figures 7 and 8, middle columns): overall, the differences mirror the zonal picture of the polarity dominance with a region of dominance of one polarity being also a region of this polarity being more distinct: namely, in the vicinity of the ACC and south and southwest of Australia, where cyclones dominate, they have a larger amplitude (several 10%), longer lifetimes (several 10%) and are larger in diameter (10–20%). The intensity (amplitude over radius) is larger as well, as the larger amplitude is more pronounced than the larger diameter (several 10%). Correspondingly, where anticyclones dominate, i.e., in the southern subtropical gyres, they are similarly more distinct in these properties.

Overall, the distributions of amplitudes, diameters, and intensities (Figure 7, right column, ratios) reveal that a roughly equal number of anticyclones and cyclones exist for the average/median, i.e., the ratio of numbers of anticyclones over the number of cyclones is roughly one. In contrast, a larger number of anticyclones exists for below average amplitudes, diameters, and intensities (the ratio is larger than one), i.e., in the more quiescent areas such as the subtropical gyres. Cyclones are more numerous for above average/median amplitudes and intensities, i.e., in the dynamic areas such as along the ACC, whereas anticyclones are again more numerous for very large diameters, likely associated with the boundary currents north of the ACC.

3.4. Eddy Shape

The average eddy in the Southern Ocean is axisymmetric (Figure 9/supporting information Figures S8a, second column, black contours). The eddy edge as detected by the OW parameter clearly marks an "inner part," i.e., a core, characterized by a decreased gradient of sea surface anomalies. The highest sea level anomaly gradients are found slightly outward of the eddy core and result in a ring of intensified geostrophic

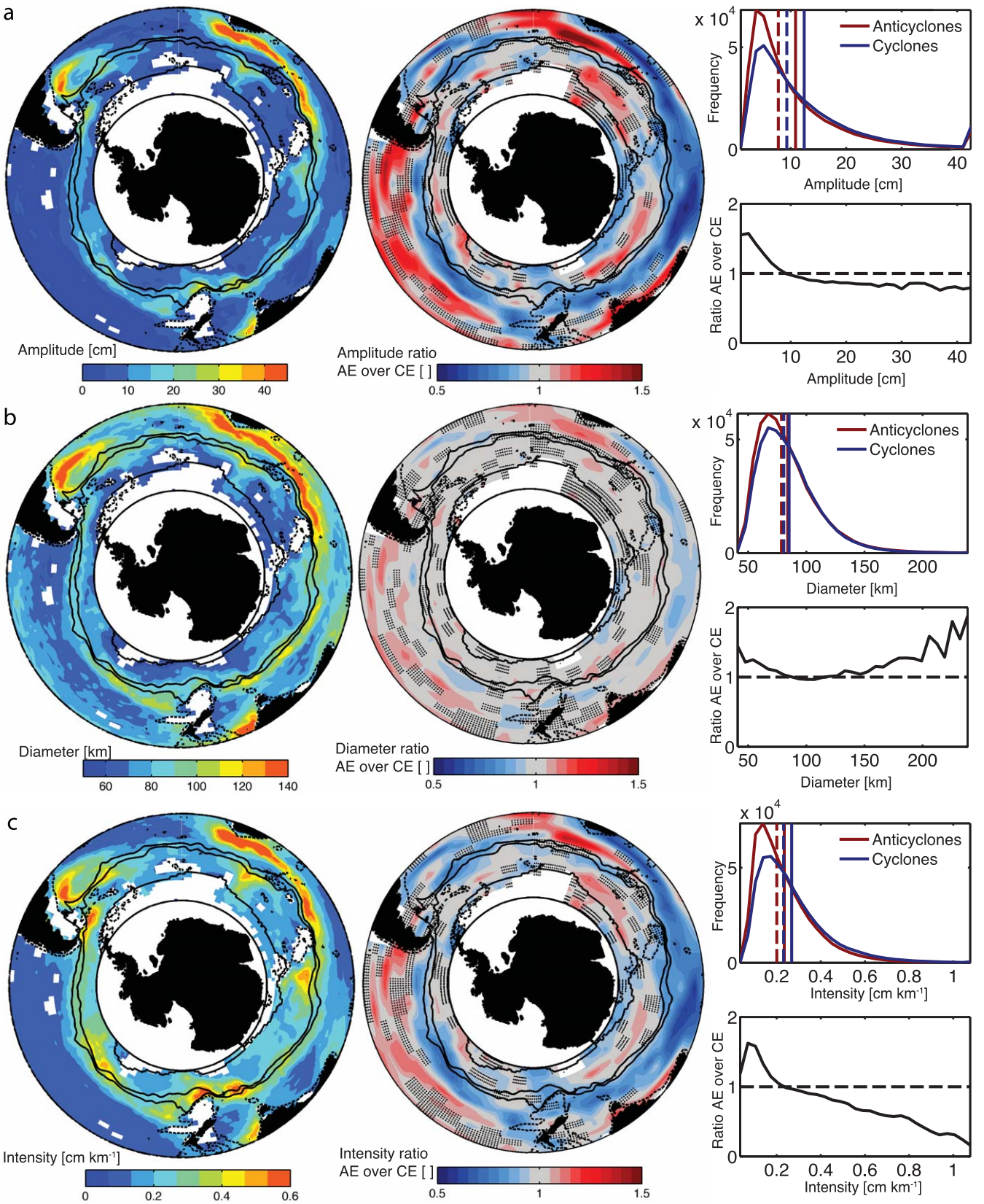

Figure 8. As Figure 7 for (a) eddy amplitudes, (b) diameters, and (c) intensities (ratio of amplitude over eddy radius); (right column) based on a 2° × 1° grid, linearly interpolated, (middle column) based on a 8° × 3° grid, linearly interpolated.

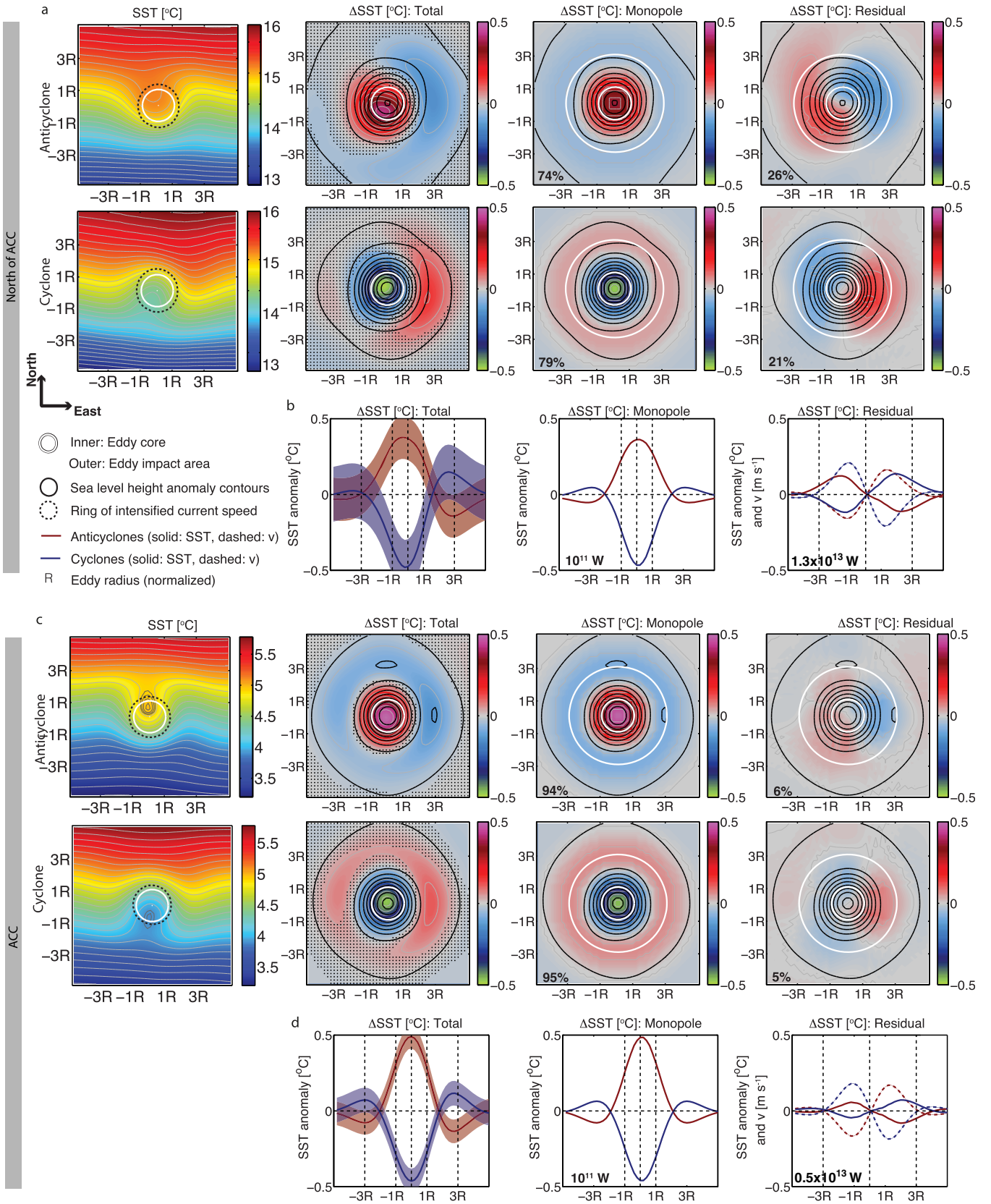
a
SST [°C]
ΔSST [°C]: Total
ΔSST [°C]: Monopole
ΔSST [°C]: Residual
North of ACC
Anticyclone
Cyclone
74%
26%
79%
21%
North
East
Inner: Eddy core
Outer: Eddy impact area
Sea level height anomaly contours
Ring of intensified current speed
Anticyclones (solid: SST, dashed: v)
Cyclones (solid: SST, dashed: v)
R Eddy radius (normalized)
b
SST anomaly [°C]
SST anomaly [°C] and v [m s-1]
10^11 W
1.3x10^13 W
c
ACC
94%
6%
95%
5%
d
0.5x10^13 W

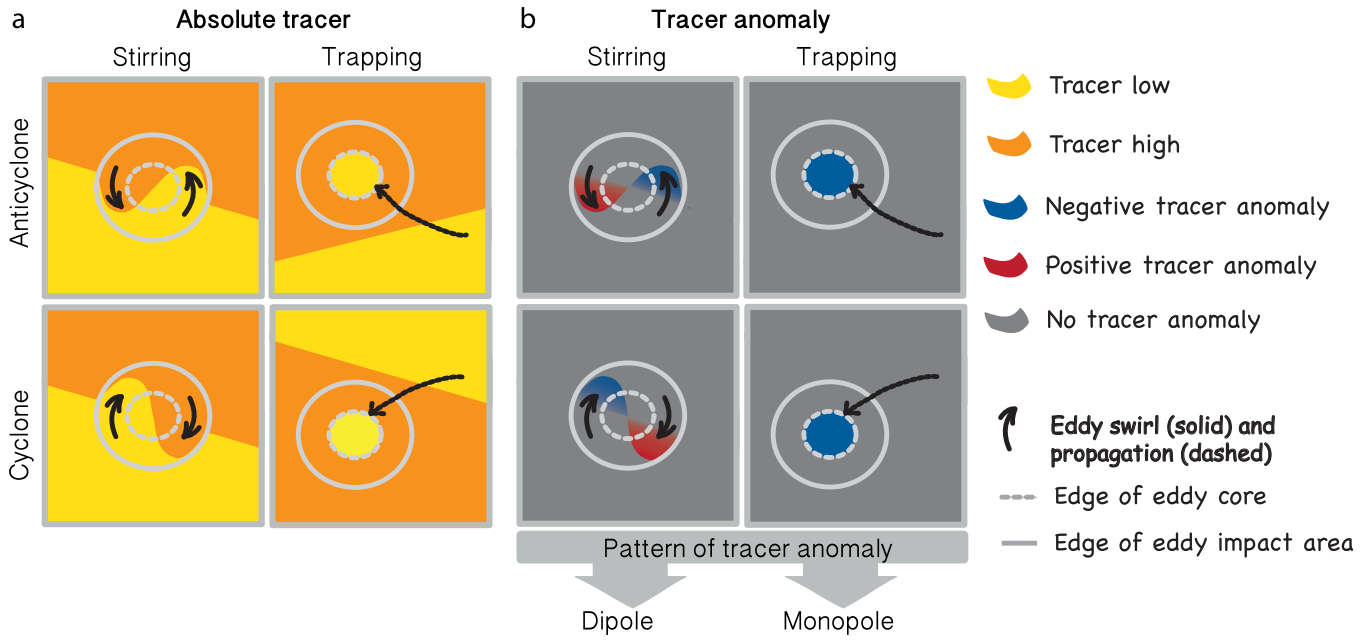

Figure 10. Cartoon illustrating the hypothetical distinction of tracer anomalies associated with eddy *trapping* and eddy *stirring* in the mixed layer. (a) Absolute tracer values in a situation of an idealized large-scale tracer gradient (for instance temperature); (b) the same situation but instead of absolute values tracer anomalies are depicted: the hypothesis is that *stirring* results in a dipole shaped anomaly whereas *trapping* results in a monopole shaped anomaly; below the mixed layer, eddy effects on tracers have a significant vertical contribution which is not the focus here.

current speeds girdling the eddy core (Figures 9a and 9c/supporting information Figure S8 first column). Closed sea level anomaly contours extend further from the center, at least twice the radius of the eddy core. A closer inspection reveals that eddies north of the ACC have closed contours of sea level anomalies beyond two of the core radii, whereas eddies associated with the ACC impact their surroundings up to two radii. The wider impact area (see section 2) and accordingly the greater "length scale of impact" for subtropical eddies is likely due to their propagation through a more quiescent sea surface height environment.

The extension of the eddies' impact beyond the OW-core becomes clear also when examining the SST anomaly related to the eddy (relative to a monthly climatology, Figure 9/supporting information Figures S8, second column, colors). Anticyclones and cyclones have positive and negative SST anomalies relative to their surroundings of several 1/10°C, respectively, where the SST anomalies are generally more pronounced in the ACC area relative to the area north of the ACC. A systematic spatial lag between the eddy and the SST anomaly exists (east-west section shown in Figure 9/supporting information Figures S8), which is smaller in the ACC than to the north of it (in agreement with *Hausmann and Czaja* [2012]). We will discuss a potential explanation for this lag based on the spatial pattern of the SST anomaly in section 4 (see also Figure 10).

The impact of the eddies extends deep into the ocean's interior (Figures 11 and 12, supporting information Figure S9). The eddy cross sections derived from the Argo floats reveal that eddies vertically extend down to 2000 m on average. This is most obvious in the density anomalies (anomalies of more than ± 0.1 and 0.2 kg m^{-3} for ACC and subtropical eddies, respectively). Temperature (anomalies of more than ± 1 and 2°C for ACC and subtropical eddies, respectively) and salinity anomalies (anomalies of more than ± 0.1 and 0.2 for ACC and subtropical eddies, respectively) are both surface intensified, with salinity opposing the

Figure 9. Average surface two-dimensional shape of eddies. (a, b) North of the Antarctic Circumpolar Current (ACC, −20 cm sea surface height contour) and (b, c) associated with the ACC; colors denote the sea surface temperature (SST) and SST anomalies relative to a monthly climatology, black contours the sea level anomaly contours (2 cm spacing); inner white circle marks the eddy's center as detected with the OW, outer white circle three eddy radii; stippling shows areas where anomalies are not significantly different from zero (*t*-test, $p = 0.01$); (left column) absolute SST, (second from left) SST anomaly, (right and second from right) SST anomaly split up into a monopole (calculated by radial averages around the eddy center) and dipole (residual); the numbers in the lower left corner show the contribution of the monopole and dipole to the pattern of the total SST anomaly (see text); Figures 9b and 9d are east-west cross sections through the eddy composite core as shown in Figures 9a and 9c; the solid line denotes the SST anomaly with the shaded error bar indicating standard error, the dashed line denotes the eddy composite meridional velocity (v); the numbers in the lower left corner show a crude estimate of the heat transport associated with the monopole (*trapping*, *drift*) and dipole (*stirring*, *swirl*) SST anomaly of the average eddy.

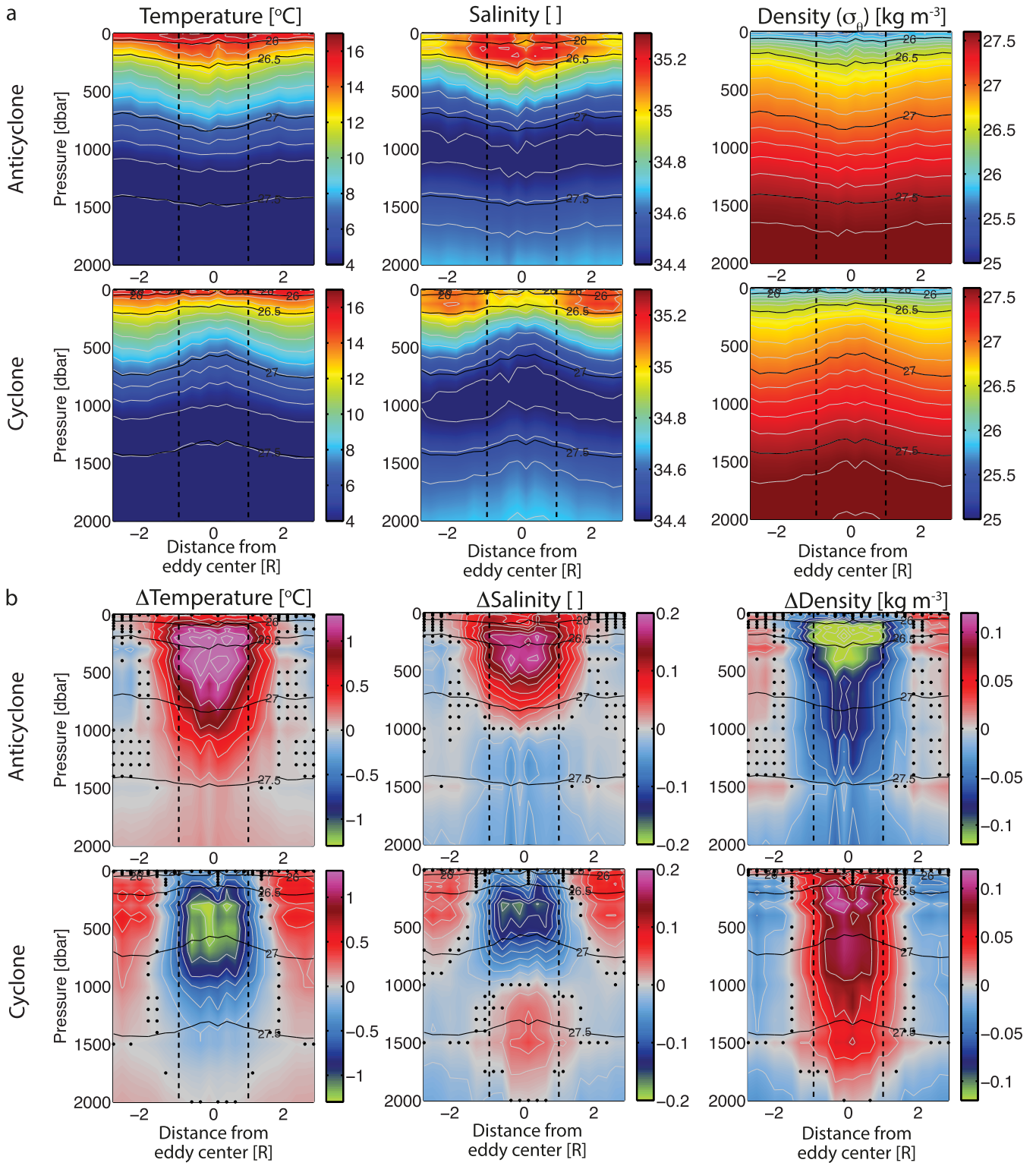

Figure 11. Average subsurface two-dimensional structure of anticyclonic and cyclonic eddies north of the Antarctic Circumpolar Current (ACC). (a) Absolute values and (b) anomalies relative to a monthly climatology; (left) potential temperature (calculated from in situ temperature); black dots mark anomalies smaller than the standard error of the mean; (middle) practical salinity; (right) potential density referenced to the surface minus 1000 kg m^{-3} (σ_0), calculated for individual profiles before averaging; temperature, salinity, and density are shown in colors and with gray contours (1°C, 0.1 and 0.1 kg m^{-3} intervals in Figure 11a, and 0.2°C, 0.02 and 0.02 kg m^{-3} intervals in Figure 11b); in each part, potential density is indicated with black contours (0.5 kg m^{-3} intervals); dashed lines mark the eddy edge (1 radius) as detected with the OW; the horizontal axis is given in normalized eddy radii (R), the vertical axis in 1 dbar ≈ 1 m.

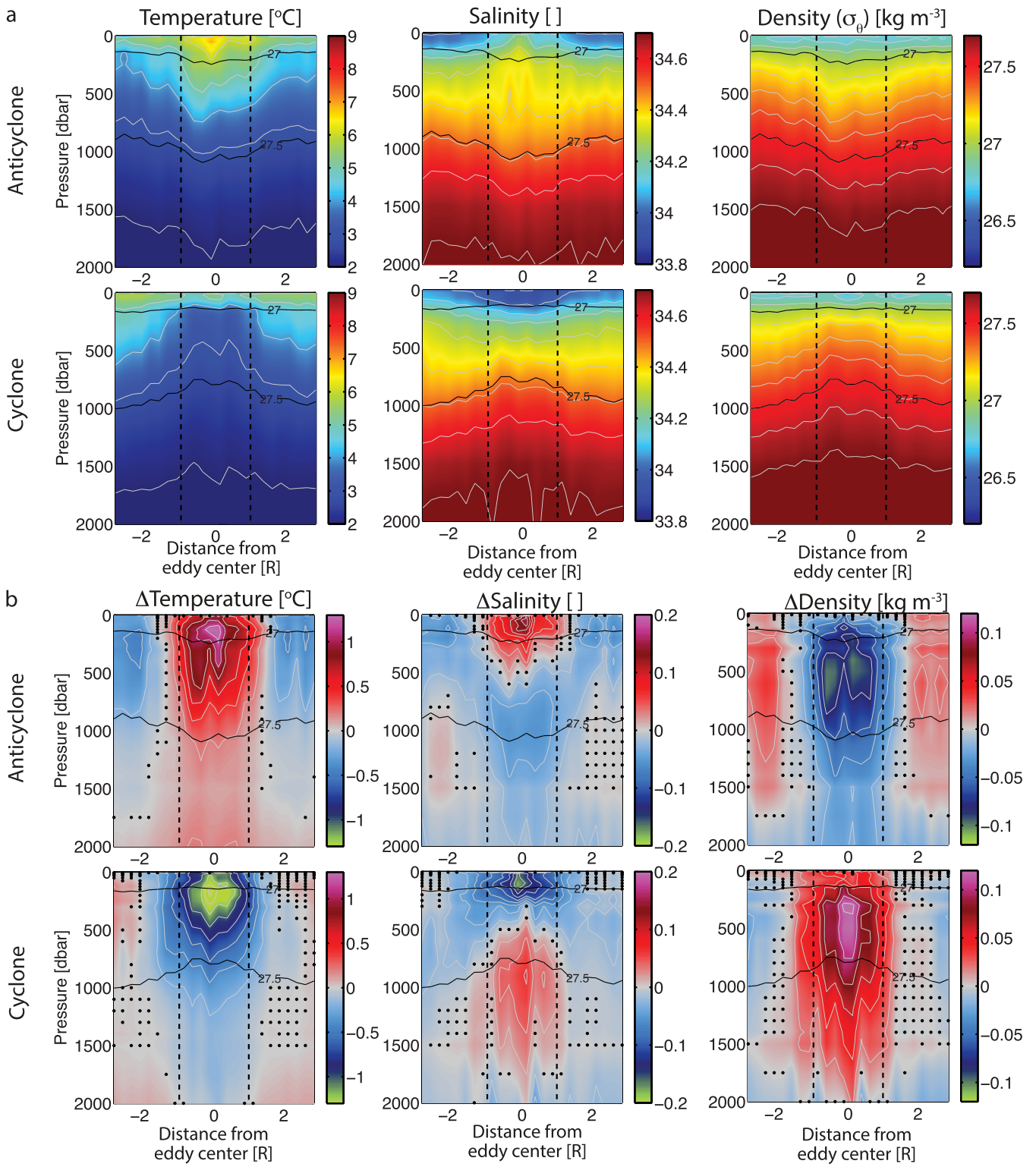

Figure 12. Average subsurface two-dimensional structure of anticyclonic and cyclonic eddies associated with the ACC; otherwise same as Figure 11 (note that the color scales are different in Figure 11a and Figure 12a).

temperature driven density anomaly in the upper ocean: cyclones tend to be cold and fresh and anticyclones warm and salty. In contrast, at deeper levels (about 500 m for ACC eddies, and about 1000 m for subtropical eddies), the salinity anomaly is of opposite sign than in the upper ocean, thus reinforcing the

density anomaly. That is, at depth, cyclones tend to be cold and salty and anticyclones warm and fresh. Temperature anomalies typically do not show such a sign switch at depth.

Several differences exist between eddies north of the ACC (subtropical) and eddies associated with the ACC. First, eddies north of the ACC show, on average, larger extrema in their anomalies than ACC eddies. Second, subtropical eddies typically have their extrema at deeper levels. Third, in some regions north of the ACC, eddies feature multiple anomaly extrema in their depth structure. In extreme cases, these anomaly maxima may be of opposite sign compared to expectations based on the polarity of the eddies. This is, for instance, the case for eddies originating south and west of Australia, where cyclones have an atypical warm and salty near-surface anomaly (in the upper 200 m, see supporting information Figure S9). Hence, with regard to eddy identification on the basis of SST [*Fernandes et al*., 2011; *Dong et al*., 2011] and concerning impacts of eddies, one cannot always relate anticyclones with positive and cyclones with a negative temperature anomaly at the surface [see also *Chaigneau et al*., 2011]. Finally, along the ACC, the depth structure of cyclones and anticyclones is similar with a first baroclinic-mode-style upper ocean intensification, whereas north of the ACC, cyclones and anticyclones often have differing depth structures with anomaly extrema at depths [see also *Chaigneau et al*., 2011]. The varying vertical structure of eddies north of the ACC compared to within the ACC especially in terms of salinity and temperature may be caused by differences in their origin water column and current structure. *Chaigneau et al*. [2011] concluded that the subsurface maximum anomalies of southeast Pacific eddies resulted from the vertically sheared boundary currents the eddies developed from. The subsurface maximum anomalies we similarly find for eddies detected north of the ACC may well be caused by this mechanism, as the majority of eddies there are associated with boundary currents.

We have discussed above the average eddy structure over two large zonal regions (eddies associated with the ACC and north of the ACC), plus the structure of a subsample of eddies (long-lived eddies north of the ACC southwest of Australia). To get some sense of the variation of the eddy structure in the Southern Ocean, the reader is referred to supporting information Figures S10–S16 where we present eddies for a selection of subregions.

The *depth-averaged* anomalies (down to 2000 m, no data are available below this level from Argo floats) appear to be similar in temperature and density for eddies within and north of the ACC (Figure 13), in spite of the different vertical structure of their anomalies. The average salinity is less clear: as it averages to zero for eddies south and southwest of Australia north of the ACC, where the upper ocean and deeper ocean anomalies of opposing sign basically cancel. In the other regions, cyclones are of either sign, and anticyclones tend to be salty. The depth-averaged temperature anomaly at the eddy center averages to about ± 0.5°C, and the density anomaly, driven by the temperature anomaly, to ± 0.05–0.010 kg m^{-3}.

The relationship of depth-averaged temperature and density anomalies of eddies and surface derivable characteristics such as intensity have an approximate linear relationship for the average Southern Ocean eddy, with a temperature anomaly of roughly 2°C at an eddy intensity of 1 m per 100 km (Figure 14). The relationship with salinity is not as clear and is approximately flat for ACC eddies due to the small to zero vertically averaged salinity anomalies. The few previous efforts to relate surface and subsurface eddy temperature and salt anomalies based on observations have not derived a comparable diagnostic [*Chaigneau et al*., 2011; *Castelao*, 2014]. It is important to note that the vertical eddy structure may vary in different places. *Zhang et al*. [2013] claim that a universal *density* structure of eddies exists: even if this were the case we want to point out to be careful to conclude from this that the temperature and salinity structure may be equally universal.

The radius as determined based on the OW parameter appears to be a reasonable proxy for the lateral extent of tracer anomalies associated with an eddy at depth (Figures 11b and 12b, and supporting information Figures S9b and S11-S16b). This is especially true for the vertically more uniform ACC eddies. Having said this, as the magnitude of the anomalies varies with depth, so does the maximum displacement of isopycnals associated with eddies. Hence, even though the radius constrains well the lateral extent of tracer anomalies, the subsurface "dynamical" extent varies with depth. ACC eddies show a somewhat conical structure with decreasing "anomaly amplitudes" with depth. North of the ACC, as noted before, the eddy structure is less universal, especially with regard to temperature and salinity.

The temperature and salinity values of the average eddy in the upper ocean differ substantially from surrounding waters. Anticyclones feature higher salinities (Figure 11/12a, middle column) and temperatures

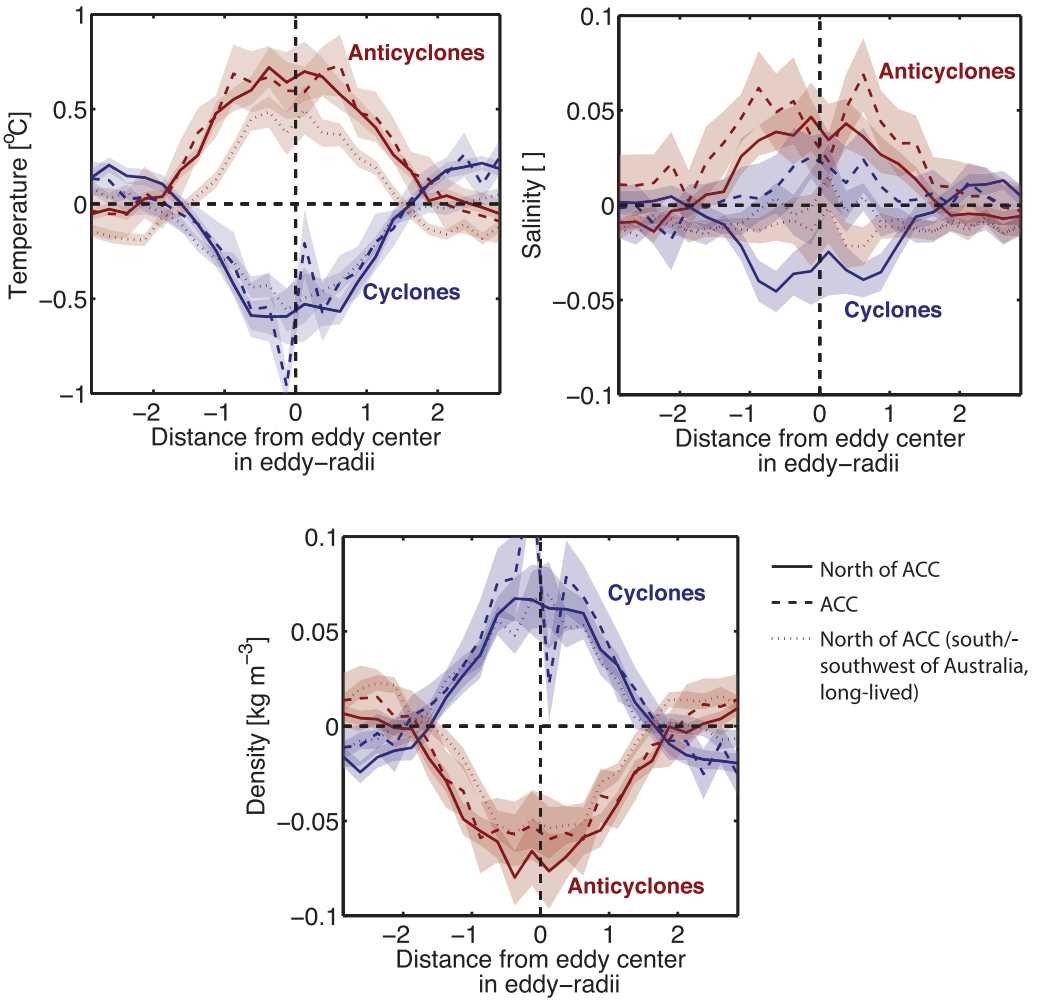

Figure 13. Depth-averaged subsurface two-dimensional structure of ACC anticyclonic and cyclonic eddies. (a) Potential temperature, (b) salinity, and (c) potential density; anticyclones in blue, cyclones in red; solid, dashed and dotted lines show eddies north of the ACC, ACC eddies and long-lived (9 months and older) eddies north of the ACC south/southwest of Australia; shading denotes the standard error of the mean.

(Figure 12a, left column) then the neighboring waters, and cyclonic eddies are saltier (supporting information Figure S9a) or fresher (Figure 11/12a) in the surface than surrounding waters. These extreme temperature and salinity values relative to neighboring waters are robust to the section we look at along the eddy (e.g., north-south or east-west, not shown). They imply closed temperature and salinity contours associated with the eddy core. This finding is supported by satellite SST (a data set independent from the Argo profiles): in the ACC area, eddies have closed SST contours related to the eddy core on average (Figure 9c, left column, dark gray contours).

Below/in the thermocline at intermediate depths (a few 100 m to approximately 1000 m), eddies show similar temperature and salinity properties as neighboring waters on the same isopycnals, but they have clearly different vertical temperature and salinity gradients and associated different layer thicknesses and stratification at these depths (supporting information Figures S17 and S18). Beyond a depth of around 1000–1500 m, vertical gradients and layer thicknesses within eddies differ little from surrounding waters in the same density class, but temperature and salinity remain vertically displaced in conjunction with displaced isopycnals, presumably due to adiabatic displacement. This is reflected in the partly reduced magnitude of eddy anomalies at these depths when analyzed in density space (supporting information Figures S19 and S20).

4. Discussion

The results lead to a number of questions, which we discuss in turn below. A first striking observation is the strong inhomogeneity in the spatial distribution of the eddies observed based on satellite altimetry. The

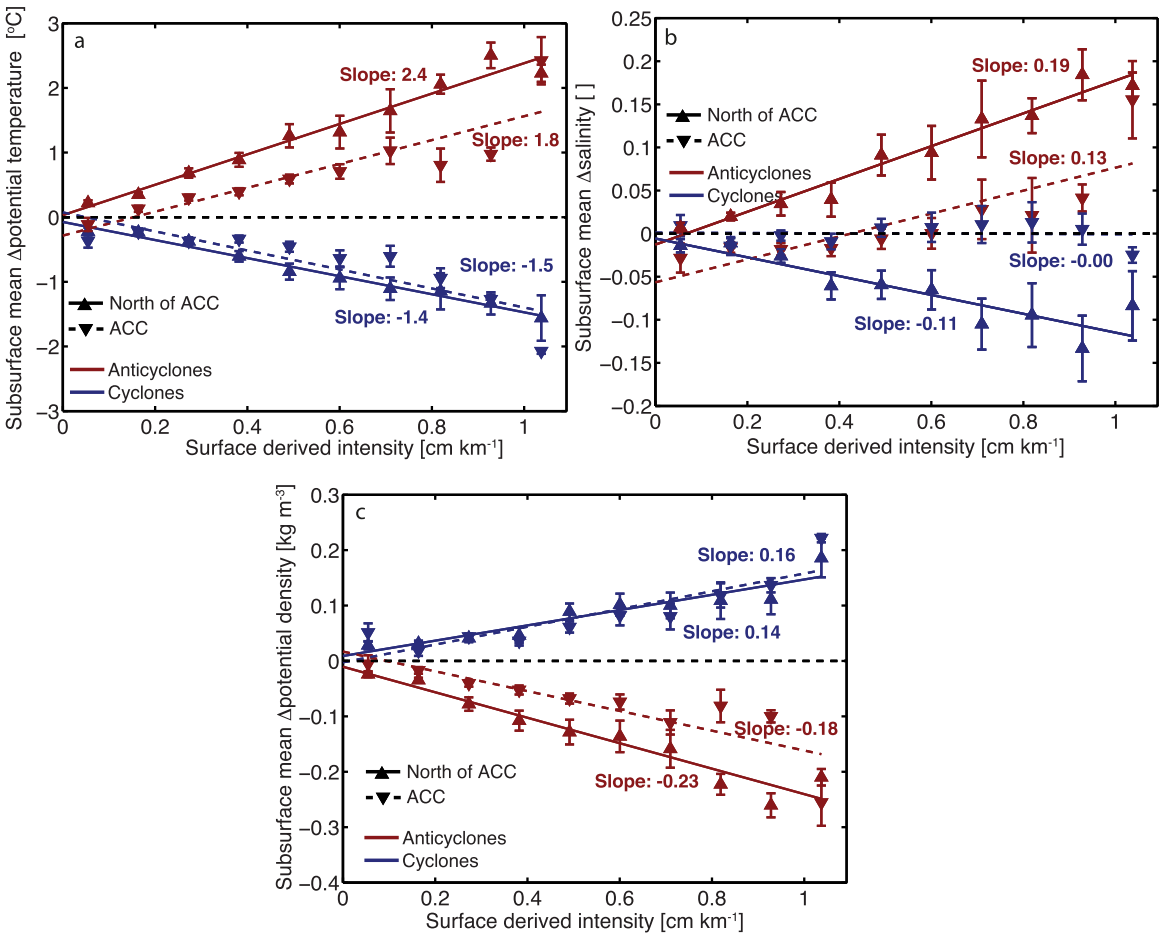

Figure 14. Relationship of surface-derived eddy characteristic (intensity) and subsurface anomalies of eddies. For (a) potential temperature, (b) salinity, and (c) potential density; binned into 10 intensity (ratio amplitude over radius) bins; all Argo profiles within the eddy core (1 eddy radius) are included; error bars denote the standard error of the mean; solid and dashed lines show a simple linear fit based on the average bins for eddies north of the ACC and associated with the ACC, respectively; slopes of linear fit are noted next to the graphs.

association of the eddies with the ACC and with the boundary currents at its northern flank is as expected, given the high levels of instabilities associated with these currents and their congruent high eddy kinetic energy [*Chelton et al.*, 1990]. However, the nearly complete absence of eddies over regions with water depths less than 2000 m is surprising. CSS11 mentioned explicitly the eddy desert in the southeast Pacific but the ones associated with plateaus along the ACC pathway have not been discussed previously.

A second striking observation is the asymmetry in the polarity of the detected and tracked eddies, as homogeneous turbulence would lead to a roughly equal number of cyclones and anticyclones. A similar large-scale pattern of polarity dominance was detected by CSS11 (their Figure 8) and is visible to some extent in *Petersen et al.* [2013, Figure 4d]. Such an asymmetry must arise either from a privileging generation mechanism, from a greater persistence of one of the polarities or from differences in the propagation paths.

The third key observation is the three-dimensional shape of the typical eddy, which shows clear signs of trapping in the upper ocean: temperature and salinity have closed contours associated with the eddy core. Based on the surface shape of tracer (SST) anomalies associated with eddies, we attribute the larger part of the eddy-associated tracer anomaly to *trapping* and a smaller part to *stirring*. Even though the maximal length scale of the *trapping* effect is given by the eddy lifetime propagation distance which is on average only in the order of 10–100 km on average, the finding suggests that eddies might be responsible for a nonnegligible amount of nonlocal meridional transport of material properties.

4.1. Eddy Distribution

The high spatial differences in the occurrence of mesoscale eddies can be the result of a number of processes: it may simply reflect differences in the rate of formation, driven by the large differences in

baroclinicity and barotropicity of the currents. An alternative explanation is that this could be the result of differences in propagation, i.e., there are no go zones and other zones where eddies accumulate. A third hypothesis is that this may reflect spatial differences in detection. We start with the third hypothesis to demonstrate that the spatial variability in eddy occurrences is likely not caused by differences in detection but reflects real spatial differences.

It is possible that the areas of low eddy coverage are actually populated by eddies, but that those eddies are smaller than the resolution of the employed sea level anomaly data, or that they are weaker and thus do not distinguish themselves clearly enough from the background. This notion is supported by the very small Rossby deformation radius over Southern Ocean bathymetrical plateaus of less than 10 km [see e.g., *Venaille et al*., 2011; *Hallberg*, 2013], which would favor the existence of small mesoscale eddies. Also the rich texture of variations seen at these scales in high-resolution SST or chlorophyll *a* observations support this notion, as well as high-resolution model simulations [e.g., *Liang et al*., 2012, Figure 9b]. Given the inability of the satellites to resolve features of *e*-folding scales below about 0.4°, i.e., roughly 20–40 km in the Southern Ocean (CSS11, Appendix A), it is indeed possible that the coarse resolution of the product underlying our detection is partially responsible for the eddy deserts. However, results by *Petersen et al*. [2013] indicate based on a 1/10° model simulation that while the eddy deserts in the Southern Ocean are indeed populated by eddies in their simulation (their Figure 4a), they existed in very low numbers only and tended to be weak.

Further support for our interpretation that these eddy deserts are real comes from the analysis of eddy kinetic energy. The eddy kinetic energy is a more integrated measure of eddies, as it includes the contribution of all motions at temporal scales less than the long-term mean and at spatial scales smaller than the large-scale circulation. Eddy coverage is highly correlated with eddy kinetic energy (Figure 6c). While satellite-derived maps of eddy kinetic energy suffer from the same resolution bias, eddy kinetic energy maps derived from surface drifters [see e.g., *Thoppil et al*., 2011, Figure 1d; *Kelly et al*., 1998] include smaller scales of sea level anomaly variability unresolved by satellites. Wherever such comparisons between satellite and drifter-derived eddy kinetic energy were done, the drifter-derived eddy kinetic energy was found to be somewhat higher than the one derived from altimetry, but the spatial pattern was the same.

Hence, we conclude that (i) if eddies occur over topographical plateaus, they are smaller (likely submesoscale) and weaker than the eddies which are the focus here and that (ii) spatial differences in detection are not likely the cause of our finding that the topographical plateaus are devoid of mesoscale eddies.

Clearly, differences in the generation can explain part of the spatial distribution of mesoscale eddies. Increased eddy numbers are strongly associated with sea surface height gradients squeezed by topography [*Sallée et al*., 2008; *Sokolov and Rintoul*, 2009b] and downstream eddy generation [*Sokolov and Rintoul*, 2009a; *Thompson et al*., 2010], such as the Drake Passage/Scotia Ridge/American-Antarctic Ridge, the Southwest Indian Ridge/Del Cano Rise/Conrad Rise, the Kerguelen Plateau, the Indo-Pacific Ridge/Campbell Plateau, and the East Pacific Rise/Pacific-Antarctic Ridge/Eltanin Fracture Zone. The ACC avoiding bathymetrical obstacles and the subsequent preferential development of eddies downstream of topography explain part of the lack of mesoscale eddies *over* topographical plateaus. If eddies form over the topographical plateaus, presumably they result in eddies close to or in the submesoscale range due to the small Rossby deformation radius, and below the detection limit of the altimetry data.

Differences in propagation pathways and lifetimes are the final mechanism that generates spatial variations in mesoscale eddy occurrences. Although, on average, the eddies do not propagate far, a small fraction does, and can generate spatial differences in eddy occurrence. For instance in the subtropical gyres, very long-lived eddies propagate westward and oftentimes dissipate only when they reach the western boundary currents [*Zhai et al*., 2010], i.e., eddy propagation is a key mechanism. But why do mesoscale eddies not leave their nurseries and propagate into the eddy deserts of the ACC region?

The topographical plateaus characterizing these mesoscale eddy deserts along the ACC are indeed in reachable distance of areas having sizable eddy populations. One explanation for the avoidance of shallow topography is that the eddies are steered directly by topographic contours (roughly equal to f/H, with f the Coriolis parameter, and H ocean depth). Eddy tracks show a close relationship with topography, indeed (see Figures 2–4b, and 5a). This behavior is consistent with the deep reaching nature of the mesoscale eddies in the Southern Ocean. Eddies have been previously found to reach deep in in situ studies (down as deep as

4000 m, e.g., *Van Aken et al*. [2003] and *Swart et al*. [2008]), so that topographic steering of the eddies is a reasonable candidate for explaining the "avoidance" of shallow topography.

Another explanation is advection, since the topographically steered nature of the ACC [e.g., *Gille et al*., 2004] makes this system of currents flow around the shallow regions, so that any eddy that is advected eastward toward these shallow regions could be swiped around these topographical features. Our data do not permit to differentiate between the last two explanations, but it is clear that topographic steering is important.

4.2. Eddy Death

There are at least four processes that cause eddies to die, i.e., (i) hitting land, (ii) transferring energy back to the mean flow, (iii) merging or splitting, and (iv) losing energy through interaction with bottom topography in the open ocean. These mechanisms have a strong spatial nature, possibly explaining why eddies generated in certain places live longer than those generated elsewhere.

A place where the topographic barrier effect is clearly important are the western boundaries of the ocean basins, as some of the very long-lived, westward propagating eddies in the subtropical gyres will hit land there, eventually leading to their death [*Zhai et al*., 2010; *Petersen et al*., 2013; CSS11]. We cannot provide evidence for this effect here as we miss a large fraction of the long-lived gyre anticyclones (they are north of our domain or leave it while they are migrating northwestward).

One process that can lead to the death of eddies by the transfer of energy back to the mean flow is the suppression of eddies caused by the shear associated with the strong currents in the Southern Ocean [*Naveira Garabato et al*., 2011; *Thompson and Sallée*, 2012]. For this process to happen, the shear of the ambient flow at the scale of eddies should be large compared to the eddies' swirl velocity [*Terry*, 2000; *Shats et al*., 2007]. With a lateral shear rate at the scales of eddies of the order of 10^{-4} to 10^{-2} s^{-1} and an eddy turnover rate of the order of 10^{-7} to 10^{-6} s^{-1}, the ratio of the two is larger than 10^2 anywhere in the Southern Ocean for most eddies, making eddies fundamentally susceptible to such shear suppression. Shear suppression may explain the ephemerality of many eddies in the eddy-generation-hot spot locations (apparent from the proximity of eddy nurseries and graveyards), i.e., the preferential death of young eddies in the dynamic regions of the Southern Ocean where large mean currents and high shear rates prevail. Also e.g., *Ferrari and Nikurashin* [2010], *Naveira Garabato et al*. [2011], and *Thompson and Sallée* [2012] have noted the suppression of eddy mixing by jets in the ACC with an energy transfer back to the mean flow.

Vortices incessantly interact, merge and split, a process that may be particularly important in the same dynamic regions where eddies are potentially suppressed by the shear of the mean flow. Eddies are presumably especially vulnerable early in their lifetime to being distorted and absorbed by more mature, intense eddies as eddies develop their maximum amplitude and diameter only about after the first 1/5 of their lifetime (supporting information Figure S7). The initial spin-up phase provides for an additional explanation why young eddies die preferentially in these regions.

The eddy energy loss via interaction with the ocean bottom may be the most important process by which ocean mesoscale energy is dissipated in the Southern Ocean and certainly a major cause of death for the long-lived eddies [*Ferrari and Wunsch*, 2009; *De Steur and van Leeuwen*, 2009; *Ferrari*, 2011; *Whalen et al*., 2012; *Nikurashin et al*., 2013]. This hypothesis is supported by the fact that surface dissipation at fronts appears to contribute only $O(10)\%$ [*Ferrari*, 2011] to the energy loss, and by the deep reaching nature of Southern Ocean eddies with significant velocities down to the ocean bottom which permits them to interact readily with bottom topography [e.g., *Schonten et al*., 2000; *Adams et al*., 2011; *Liang and Thurnherr*, 2012; *Nikurashin et al*., 2013]. The possible importance of this energy pathway in the ACC is consistent with the view that eddies are critical in the closure of the momentum budget in this region by transferring the momentum vertically to the bottom [*Johnson and Bryden*, 1989].

Further support for the importance of the eddy-bottom topography interaction mechanism comes from the tendency of eddies to lose integrated energy when they propagate onto shallower topography (Figure 5b). The fact that both amplitudes and diameters decrease precludes vortex squeezing as an alternative explanatory mechanism (not shown). This observation indeed could be an indication for an energy sink of the eddy associated with the ocean floor as it hits a subsurface topographical obstacle. In combination with the topographical steering effect, the energy loss of eddies when interacting with bottom

topography would contribute to an explanation for why prominent eddies do not occur over topographical plateaus along the ACC.

4.3. Polarity Dominance

The dominance of one eddy polarity over the other (Figure 6b) may simply reflect polarity-related biases in our detection algorithm. Therefore, we need to exclude this possibility before proceeding. One check is the analysis of the third moment of the distribution of sea level anomalies, i.e., its skewness [*Thompson and Demirov*, 2006]. It turns out that the pattern of polarity dominance we find from our Lagrangian approach agrees largely with this metric (Figure 6d), supporting our eddy census-based results. An important exception is the southern part of the Southern Ocean, where we identified a dominance of anticyclones whereas the skewness hints toward a dominance of cyclones (dots clustering at 1 at the *y* axis in Figure 6d). However, we detected only a small number of eddies in this area altogether, which makes a ratio, such as the one we consider here (coverage by anticyclones over total coverage by eddies), less trustworthy.

As mentioned before, the dominance of one eddy polarity over the other can be due to any combination of (i) differences in formation, (ii) differences in spatial segregation during their propagation, and (iii) differential lifespan and death. We discuss each of these mechanisms in turn, starting with the formation and lifespan/death mechanisms.

The differential spatial pattern of major formation locations and lifespans of anticyclones and cyclones clearly contributes to the overall pattern of polarity dominance (mechanisms (i) and (iii)). In fact, the strong similarity of polarity dominance in formation areas and lifespans with those areas of the polarity dominance suggests that these processes are the dominant mechanisms leading to the dominance of either anticyclones or cyclones (Figure 6b, supporting information Figure S4b, and Figure 7, middle column). The subtropical regions, especially the South Pacific stand out as areas of dominance of anticyclon formation. And so does the region south of the ACC, although the dominance of anticyclones south of the ACC is less robust due to the small number of detected eddy events. The ACC is an area of about equal numbers of anticyclone and cyclone generation.

The areas of nurseries where anticyclones are dominant are already apparent in the maps not weighted by lifespan, but the areas of higher numbers of anticyclone formation become even more apparent when these numbers are weighted by the eddies' lifespan (compare supporting information Figures S4b and S4c). That the pattern of anticyclonic dominance in eddy birth numbers becomes clearer when weighted by eddy lifespan means that more anticyclones form in these areas, and that they also live longer than the cyclones (see also Figure 7, middle column). In contrast, the dominance of the cyclones emerges in the ACC region only when the formation numbers are weighted with the lifespan (compare supporting information Figures S4b and S4c). Thus, the total number of cyclones generated in this region is not necessarily larger than that of the anticyclones, but the cyclones die not as quickly. Exceptional areas are the east Atlantic and east Indian Ocean: in the east Atlantic, anticyclonic dominance becomes apparent only when birth numbers are weighted by lifespan (i.e., the long-lived Agulhas rings cause the anticyclonic polarity dominance), whereas in the east Indian Ocean cyclonic dominance begins to show only when weighted by lifespan. To both of these exceptional areas, eddy propagation pathways form a major contribution, i.e., mechanism (ii). In the following, we will first provide a few potential causes for differences of anticyclone and cyclone formation and lifespan, and second will discuss the role of eddy propagation pathways.

A rather obvious cause of a systematic regional polarity dominance in the formation is the symmetric pinching off of eddies from fronts. This mechanism is likely responsible for the pattern of polarity dominance associated with intense currents, such as the Malvinas-Brazil Confluence or the dominance of cyclones at the northern flank of the ACC.

A further contribution to differential formation may arise from wind forcing that could favor one of the polarities [*Liang et al*., 2012; see also CSS11]. *Griffa et al*. [2008, Figure 3a] computed (anti)cyclonic motion in the global ocean from surface drifters and found a dominance of small-scale anticyclonic loopers ($O(100)$ suppress line break between number and unit km and less, their Figure 4) at the poleward side of the subtropical gyres. These loopers are correlated with (high frequency) wind forcing and hypothetically caused by resulting Ekman transports in the ocean boundary layer (i.e., inertial oscillations). It is unclear if mesoscale

features were preferably anticyclonic when generated by wind forcing, hence if wind forcing could cause the excess anticyclones formed in the subtropical gyres.

One reason for a longer lifespan could be that when eddies are born, one polarity has a higher integrated eddy kinetic energy than the other. Indeed, cyclones tend to show a larger initial integrated kinetic energy see supplementary material Figure S7, part a-4, hence a larger initial integrated kinetic energy leading to a longer lifespan could be an explanation for the cyclonic dominated areas. Yet another contribution could come from differing characteristics that make eddies more or less prone to energy drainage over their lifetime. For instance, the greater intensity of cyclones makes them less vulnerable in the ACC to the aforementioned shear suppression, permitting them to survive longer. The causes for asymmetries of anticyclones and cyclones are unclear and are subject to ongoing research also in fluid dynamics [e.g., *Arai and Yamagata*, 1994; *Nycander*, 1994; *Cenedese and Linden*, 1999; *Hakim et al*., 2002; *Frisius*, 2003; *Graves et al*., 2006; *Ponomarev et al*., 2009; *Moisy et al*., 2011; *Perret et al*., 2011; *Badin*, 2013; *Heinloo et al*., 2012], with suggestions that longevity of anticyclones is favored by anticyclones being more stable and less prone to Rossby wave dispersion. In contrast, a potential contribution favoring cyclones could arise from centrifugal forces acting differently for anticyclonic and cyclonic eddies. For example, thinking about it very simplified, one could expect the outward pressure force for anticyclones at the air-sea interface to weaken the eddies and the contrasting inward pressure force for cyclones at the sea surface to strengthen the eddies, making anticyclones more vulnerable and cyclones more robust toward "extrinsic perturbations."

A further process contributing to different anticyclonic and cyclonic lifespans could be differences in the rate of energy drainage by air-sea interactions [*Shuckburgh et al*., 2011; *Byrne et al*., 2015]. Air-sea interaction may lead to an asymmetric energy loss of anticyclones and cyclones as the positive temperature anomaly of anticyclones may be reduced via sensible and latent heat fluxes more efficiently than the negative temperature anomaly of cyclones. If cyclones gain heat at the surface via air-sea interactions, the water stability increases as the surface water becomes warmer and hence lighter, subsequently damping vertical mixing. In contrast, if anticyclones lose heat to the atmosphere, the surface cooling destabilizes the water column, leading to increased mixing, which in turn facilitates further energy loss at the surface [*Van Aken et al*., 2003]. As this effect makes anticyclones more prone to dissipation of their temperature anomaly, it may help to explain the quicker death of anticyclones in the ACC region, where cyclones dominate. The potentially emphasized role of this mechanism in the ACC regions is consistent with the eddies having larger SST anomalies there [*Hausmann and Czaja*, 2012; *Frenger et al*., 2013].

The final mechanism to consider which contributes to polarity dominance in an area are differences in the propagation pathways between anticyclones and cyclones (mechanism (ii)), especially since the intrinsic meridional propagation of cyclones is opposite that of the anticyclones [*Cushman-Roisin and Beckers*, 2011; CSS11]. As shown in section 3, our observed eddies only partially follow this intrinsic propagation (supporting information Figures S6b and S6c). The anticyclones meet their expectation of an equatorward deflection only in the subtropical gyres, while the cyclones show the expected poleward propagation mainly in the eastern Indian Ocean north of the ACC. Nevertheless, we can find prominent examples of propagation as cause for polarity dominance: the broad zonal band of cyclones at the northern flank of the ACC in the Indian sector is presumably due to the very long-lived cyclones originating from the Australian coast and propagating southwestward toward the ACC (hypothetically Tasman Leakage or Tasman Outflow cyclones) [*Speich et al*., 2002; *Ridgway and Dunn*, 2007]. Relatively few eddies are generated in this region along the propagation path of these cyclones (supporting information Figure S4a), hence the long traveled cyclones, even though they do not occur overly frequent, dominate the absolute number of eddies. Similarly, the anticyclones propagating northwestward from the South African coast (the Agulhas rings) propagate far into the Atlantic into areas of little eddy generation, thus dominating absolute eddy numbers there.

4.4. Eddy Trapping Versus Stirring

A fundamental question associated with the role of eddies for the large-scale transport of heat and material properties is how eddies affect tracers: it is unclear to which degree eddies are coherent vortices, trapping fluid properties in their interior and transport them great distances, the extent they mix waters due to their rotation (stirring), and to what degree eddies are merely distorting the environmental conditions through which they are propagating, i.e., acting like a wave and not causing a net transport [e.g., *Chelton et al*., 2011b; *Morrow and Le Traon*, 2012]. It is often argued that typically eddies (at high latitudes) show rotational speeds much larger

than propagation speeds (e.g., CSS11), which is an indication for coherent vortices which can trap fluid [*Flierl*, 1981]. Here we discuss the *trapping* and *stirring* effects based on the three-dimensional shape of the eddies in combination with eddy temperature and salinity characteristics. This combined assessment of eddy dynamical properties and eddy effects on tracers can provide answers to the question if eddies *trap* or *stir*.

Of particular interest is the eddy's SST pattern, since we know it for nearly every eddy we identified and tracked, while we have for only 1.5% of eddy instances a profile available within the eddy core (within one eddy radius from the eddy center) to reconstruct the ocean interior distribution of the eddies (but still more than 1.3×10^4 profiles overall). The number of profiles increases to more than 10^5 for profiles surfacing at a distance of three eddy radii from the eddy center. The mean SST pattern consists primarily of a monopole (Figure 9, supporting information Figure S8). In order to analyze the nonmonopole part in more detail, we subtract the monopole component from the total SST composite pattern, with the monopole having been computed by taking the radial average relative to the eddy's center (similar to *Hausmann and Czaja* [2012] who separate the east-west asymmetry). The residual pattern (Figure 9, supporting information Figure S8, right column) shows a surprisingly symmetric dipole with its maximum and minimum in the peripheral area of the eddy reflecting the direction of rotation, i.e., anticlockwise for anticyclones and clockwise for the cyclones. The relative contribution of the monopole and dipole components varies considerable between the different regions. In the ACC region, more than 90% of the variance of the pattern of the SST anomaly associated with eddies is explained by the monopole (within the eddy impact area, marked with a white circle in Figure 9, for calculation see equation (2)). In contrast, the dipole is more prominent north of the ACC [*Hausmann and Czaja*, 2012], explaining 20% to up to almost 90% of the variance of the eddy SST anomaly there.

We interpret these patterns as the result of two distinct mechanisms illustrated in Figure 10, i.e., *trapping* generating a monopole pattern, and *stirring* leading to a dipole, as the eddy's swirl distorts the large-scale SST gradient within its peripheral area (as noted to be the case for chlorophyll *a* by *Chelton et al*. [2011a]). The larger contribution of the monopole pattern in the ACC region compared to the area north of it is consistent with eddies exhibiting higher swirl velocities and accordingly being more likely to be able to trap fluid. In contrast, the dominance of the dipole pattern to the north of the ACC is likely due to the stronger large-scale SST gradient relative to the width of the eddies (see section 3.4). Thus, the environmental conditions in combination with the eddies' larger length scale of impact (or "mixing length scale") may well result in the larger dipole signal. The superposition of the monopole and dipole pattern, which we attribute to *stirring* and *trapping* may cause an apparent lateral shift between sea level height anomalies and tracer anomalies as noted by *Hausmann and Czaja* [2012] (see e.g., supporting information Figure S8b, left).

The *trapping* and *stirring* effects are not completely independent. An additional aspect of eddies impacting their surrounding tracer field is that eddies perturb the tracer field as they propagate through it with their intrinsic phase speeds (CSS11). Thus, the trailing (roughly eastern) side of the eddy features a smaller tracer anomaly as it distorts an already perturbed tracer field, whereas the leading (roughly western) side of the eddy impacts an assumed unperturbed one resulting in a larger tracer anomaly. As the eddy is propagating, this leading side anomaly might be partially entrained into the eddy core and get trapped, at least temporarily. The contribution of this effect to the (monopole) SST pattern versus the contribution of waters stemming from the eddies nursery is difficult to quantify even in models, even though a few approaches to assess the permeability of an eddy exist [*Williams et al*., 2012; *Beron-Vera et al*., 2013].

The fact that the average absolute value of the SST signal related to the eddy core is larger than the SST of ambient waters, i.e., closed SST contours associated with the eddy core exist (Figure 9c), supports the hypothesis that the water in the eddy core is at least to some extent originating from a region of different SST, hence that the eddy partially traps water. Likely, the SST anomaly in the eddy core is due to a superposition of the eddy retaining waters temporarily and continuous entrainment of new waters from the eddy's surroundings.

The vertical structure of eddies supports the notion of eddies as coherent features and the importance of *trapping* in the upper ocean (Figures 11a and 12a, supporting information Figure S9a). In particular, the extreme values of salinity and temperature inside the eddies relative to surrounding waters in the upper ocean above the thermocline, and the associated closed temperature and salinity contours can only be generated by eddy *trapping* (see section 3.4).

The ability for eddies to trap at deeper levels is less evident in our analysis, especially since below the surface ocean (down to approximately 1000 m or so), temperature and salinity contours are not necessarily

closed any more. However, the vertical gradient of temperature, salinity, and stratification is clearly different from neighboring waters. The thickness of temperature, salinity, and density layers is increased for anticyclones and decreased for cyclones, hypothetically caused by isopycnal layer thickness advection, with a contribution by downward diapycnal diffusion of the near-surface anomaly. Downward diffusion of the near-surface anomaly and adiabatic heaving/depressing of isopycnals cannot be the only reason as for instance the net negative sea level anomaly of cyclonic eddies south/southwest of Australia must be caused by the deep heavy density anomaly which overcompensates the near surface light density anomaly. We cannot assess to which extent the anomalies of eddies below/in the thermocline are due to *trapping*. Our inability to assess the role of trapping at deeper levels is congruent with the mixed results obtained by previous modeling studies with a realistic setup: *Nakano et al*. [2013] concluded based on dye and particle release experiments in the Kuroshio region that eddy trapping efficiencies are high above and within the thermocline, but that leakage occurs increasingly at deeper levels. In contrast, *Donners and Drijfhout* [2004] particle release study in the Agulhas region shows that Agulhas rings were leaky in the surface (mixed layer) due to a secondary circulation, while the ability to trap was high below the mixed layer down to nearly 1 km.

Further down in the water column (down to 2000 m and beyond), eddies likely no longer trap material properties. In fact, our results suggest that the anomalies of eddies can be explained mainly by pure compensating adiabatic vertical displacements of the isopycnals. The compensating displacements of isopycnals which in the case of cyclones heave up waters from below, and vice versa for anticyclones, likely causes at least to some degree the sign switch of the salinity anomaly between the upper and the deeper ocean (at about 500 m depth for ACC eddies, Figure 12). In the ACC area, the salinity increases with depth, hence waters heaved up are more saline. North of the ACC, Antarctic Intermediate Water is associated with a subsurface salinity minimum, i.e., salinity decreases down to depth of roughly 1000 m. Eddies in this region show the salinity anomaly sign switch below 1000 m where the salinity increases again (Figure 11b, supporting information Figure S9b). The temperature anomalies do not switch sign with depth as the absolute temperature decreases with depth, both in the ACC area and north of it.

The eddy core with high trapping ability presumably coincides with the area of solid body rotation [*Oh and Zhurbas*, 2000; CSS11], as it is enclosed by a ring of maximum rotational speed of the eddy (CSS11, Figure 9, supporting information Figure S8). The swirl velocities then level off beyond the eddy core with a relatively large tail [*Oh and Zhurbas*, 2000]. In this peripheral area, continuous exchange may take place with the surrounding waters the eddy propagates through. This idea is supported by *Early et al*. [2011] whose results based on idealized model simulations show a strong trapping ability of an eddy within the zero vorticity contour in addition to a continuous exchange of fluid with the surrounding at the eddy's periphery. In the real ocean, individual eddies have been observed which appeared to be good in trapping: for instance *Lehahn et al*. [2011] showed that an Agulhas ring featured a patch of increased chlorophyll *a* over months, and *Ansorge et al*. [2009] found an anticyclonic eddy south of the Polar Front with a biological composition which was typical for the region the eddy originated from, which was north of the Polar Front. Yet indications exist that the ability to trap fluid in their cores varies greatly between eddies and only very few trap perfectly (e.g., *Beron-Vera et al*. [2013], based on surface data only).

4.5. Eddy Transports

It is important to refine eddy transport estimates based on eddy tracking [e.g., *Dong et al*., 2014; *Zhang et al*., 2014a, 2014b], where oftentimes perfect eddy trapping is assumed down to a certain depth and the essential question of the efficiency and/or depth structure of *trapping* is not critically discussed. The frequently applied diagnostic of "nonlinearity" as dominance of swirl over propagation speed [*Flierl*, 1981; *Chelton et al*., 2011b], or closed contours of potential vorticity, may be a reasonable indicator for *trapping* in the upper ocean but not necessarily for deeper levels [*Nakano et al*., 2013].

Irrespective of the open questions associated with eddy *trapping*, we will provide a rough estimate of the eddy heat transports due to *stirring* (F_s, dipole contribution) and *trapping* (F_t, monopole contribution) within the mixed layer. Following the approach by *Hausmann and Czaja* [2012], F_s is estimated as

$$F_s = \rho_0 c_p h_m \int_0^{L_e} \langle v_g' \rangle \langle T' \rangle \mathrm{d}x, \tag{3}$$

with a reference density of $\rho_0 = 1025$ kg m^{-3}, a specific heat capacity of $c_p = 4000$ J kg^{-1}K^{-1}, a mixed layer depth of $h_m = 100$ m, and an eddy scale of $L_e = 100$ km. v_g' and T' are the eddy meridional geostrophic

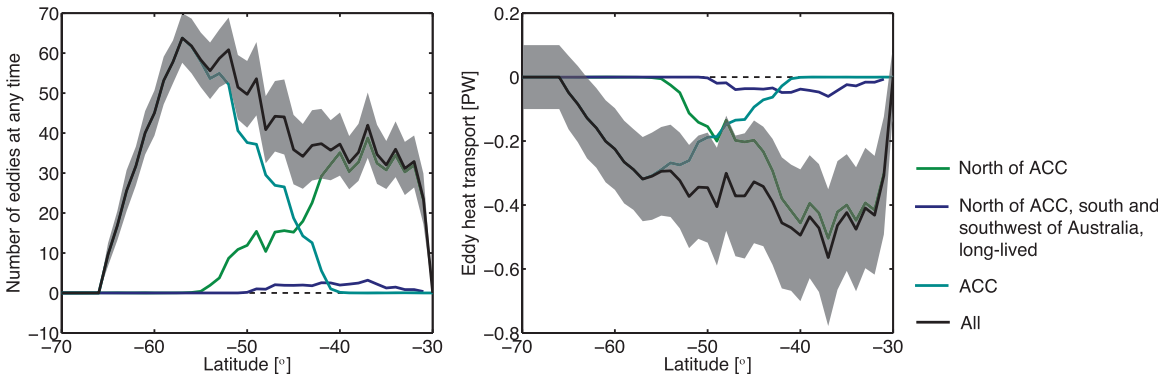

Figure 15. Upscale estimate of eddy heat transport. (a) Eddy numbers and (b) associated heat transport due to *stirring*; the *trapping* effect is not considered here as it is highly uncertain; for all eddies (black), eddies associated with the ACC (light blue), eddies north of the ACC (green), and long-lived (9 months and older) eddies north of the ACC in the east Indian Ocean (blue); the latitude bin width is 1°; black shading indicates the uncertainty due to temporal variation of eddy numbers (one standard deviation, no other error source is considered here).

velocity and temperature anomalies, with $\langle\rangle$ denoting the eddy composite. F_t is calculated as in equation (3), but with the eddy propagation velocity v'_p replacing v'_g. That is F_t and F_s are calculated the same except for a different velocity: v'_g denotes the geostrophic meridional velocity across the eddy (Figures 9b and 9d, right). v'_p is assumed to be uniform throughout the eddy, namely the average cross-frontal (not necessarily meridional) propagation speed of eddies relative to the mean flow, estimated to be of the order of 10^{-3} m s^{-1} by *Hausmann and Czaja* [2012], an order of magnitude smaller than the propagation speed of eddies as derived directly based on eddy tracks.

The resulting estimate of heat transport for individual eddies associated with *stirring* (*swirl*, dipole, 10^{12} to 10^{13} W) is 1–3 orders of magnitude larger than the estimate for heat transport associated with *trapping* (*drift*, monopole, 10^{10} and 10^{11} W, see Figures 9b and 9d, right and second from right). The larger effectiveness of *stirring* is due to the much larger swirl velocity (v'_g, order of 10^{-1} m s^{-1}) than eddy propagation velocity (v'_p, 10^{-3} m s^{-1}). The dominance of the swirl velocity over the propagation velocity overwhelms the generally much larger trapped SST anomaly compared to the stirred SST anomaly. This result is in agreement with *Hausmann and Czaja* [2012].

The southern part of the Southern Ocean experiences a net heat loss and fresh water surplus. Eddies are thought to be important for the meridional transports of buoyancy. Almost 100 eddies reside in between the two major fronts of the ACC (Polar Frontal Zone) at any time, which results in an integrated transport of close to 10^{14} and 10^{13} W for *stirring* and *trapping*, respectively, i.e., a combined transport of the order of 0.1 PW. A similar number of eddies resides in a 1° latitude bin. Figure 15 shows the eddy numbers (a) and resulting eddy heat transport (b) with latitude, based on 1° bins with approximately 100 km per latitude bin. We assume this bin spacing to be representative for the spatial scale of the eddy heat transport. The order of 0.1 PW is in agreement with previous results (see summary in *Gille* [2003], Table 1) and could account for the heat lost to the atmosphere southward of the Polar Front [*De Szoeke and Levine*, 1981].

Eddy numbers are largest near 60°S (Figure 15a), in contrast the southward eddy heat transport peaks around 40°. This shift of the latitude of maximum eddy numbers versus maximum eddy heat transport is due to the larger *stirring* contribution of eddies north of the ACC. As *trapping* is estimated to be small, it does not contribute substantially to the meridional eddy heat transport. Qualitatively, the variation of the eddy heat transport with latitude due to *stirring* matches rather well estimates based on model simulations [*Jayne and Marotzke*, 2002; *Volkov et al*., 2008; *Griffies et al*., 2015], in contrast to the eddy heat transport based on the *trapping* effect as estimated by *Dong et al*. [2014] (their Figure 4a, presumably based on a much larger eddy propagation velocity than used here). The *trapping* induced heat transport is very uncertain as first, it is unclear how efficient eddies *trap* and second, the magnitude of the cross-frontal propagation velocity v_p of eddies is likely not conclusive, for instance it may vary in space.

Even if v_p is consistently two orders of magnitude smaller than v_g, *trapping* may not be negligible as noteworthy differences exist between the process of *stirring* and *trapping* in the context of eddy transports. First, the spatial range of *trapping* may be larger than that of *stirring*: *stirring* is constrained to the spatial scale of one to several eddy radii, whereas the spacial scale of *trapping* potentially can be much larger (nonlocal),

i.e., at the scale of the distance eddies propagate over their lifetime which is 10–100 km on average. Even if *trapping* is limited to scales of 10–100 km for the majority of eddies, long-distance transports associated with *trapping* certainly exist, such as found by *Lehahn et al*. [2011] for an Agulhas ring. Also, *trapping* may be significant if the eddy crosses a major front. The occurrence of *trapping* is of interest not only for temperature and salinity considered here but also for biogeochemical tracers. For instance the Southern Ocean is a high nitrate area whereas nitrate gets depleted toward the subtropical gyres. The contribution of nonlocal transport of nutrients by eddies into the subtropical gyres is under debate [e.g., *Oschlies*, 2002]. Second, *trapping* can result in an upgradient tracer transport, whereas *stirring* always leads to downgradient transport. The intrinsic equatorward deflection of warm salty anticyclones (and vice versa for cyclones) would hence lead to an upgradient transport in the quiescent subtropical regions of the ocean. Finally, the relative contribution of *trapping* compared to *stirring* increases with depth [*Hausmann and Czaja*, 2012]. The reason being that the swirl velocities which drive the *stirring* transport decrease with depth, in accordance with decreasing density anomalies. In contrast, the velocity an eddy is propagation at is not affected by the decreasing eddy density anomaly and is the same throughout depth. In addition, the maximum temperature and salinity anomalies of eddies are located not necessarily within the mixed layer.

We try another crude estimate by considering depth integrated lateral heat transport down to 2000 m. The depth-averaged temperature anomalies result in an anomaly similar to the one observed at the surface (Figure 13a), hence with $h_m = 10^3$ instead of $h_m = 100$ m, the transport for an individual eddy due to *trapping* becomes an order of magnitude larger (10^{11} to 10^{12} W). This is supporting the previous finding that including deeper eddy transports may result in an order of magnitude larger estimates [*Walkden et al*., 2008]. If the depth-averaged swirl velocity was an order of magnitude smaller than the surface velocity (which would be a rather strong decrease), and assuming no change in the shift of temperature anomaly and swirl velocity, the decrease of the swirl velocity would cancel the increase of the integration depth, and the resulting transport due to *stirring* would stay at the order of 10^{12} to 10^{13} W. *Treguier et al*. [2003] find the depth integrated heat transport of Agulhas rings due to *trapping* dominant in a model simulation. Also, it appears rather unclear which propagation velocity of eddies is appropriate to use for the calculation of *trapping* transports: assuming a propagation velocity of an order of magnitude larger than used here would make the heat transport due to *trapping* comparable in magnitude to *stirring* transport.

5. Summary and Conclusions

We provide here the first regional study of mesoscale eddies in the whole Southern Ocean based on satellite and Argo float observations and a semi-Lagrangian approach (i.e., "following eddies over time"). Our data cover more than a decade and include the vertical structure of the eddies. By tracking more than 10^5 eddies over their lifetime, we assembled a very rich and detailed eddy data set for the area between 30°S and 65°S as resolved by Aviso altimetry data, i.e., with approximate minimum diameters of 50 km at 65° and 100 km at 30°. We examined the spatial patterns of eddy coverage and properties, and differences between anticyclones and cyclones. Our major findings are summarized schematically in Figure 1b.

The spatial coverage of the Southern Ocean by mesoscale eddies varies substantially as anticipated from maps of eddy kinetic energy. The ACC and western boundary currents are covered by eddy cores more than 15% of the time reaching more than 25% in some areas. These numbers double to triple if one considers not only the eddy core (area of one eddy radius) but also its impact area (two to three eddy radii), i.e., adding the "peripheral area." The dynamic areas in the Southern Ocean are also regions of both high rates of eddy formation and eddy death, which is consistent with the average moderate lifetime propagation distances of the order of 10–100 km.

Eddy deserts [*Henson and Thomas*, 2008; CSS11] are the southeast Pacific, an area of very deep winter mixed layers, and waters over topographical plateaus along the ACC pathway. We hypothesize that these latter eddy deserts are not only due to the ACC advecting the eddies around these plateaus but also due to direct topographical steering of eddies and a rapid energy loss of eddies propagating onto shallower topography.

By determining coherent regions of polarity dominance, we refined the findings of CSS11. Regions of polarity dominance show a zonal pattern to first order: the southern subtropical gyres are generally dominated by anticyclones, whereas the northern flank of the ACC is dominated by cyclones. This pattern agrees well with the skewness of the sea level anomalies variability [*Thompson and Demirov*, 2006]. The distribution of

polarity dominance may be critical for integrated eddy effects, as anticyclones and cyclones oftentimes show antisymmetric tracer anomalies. Mechanisms playing certainly a role for the emergence of the polarity dominance pattern are the pinching off of eddies on either side of fronts or jets, and the migration of eddies, such as distinct cyclones forming in the south and west of Australia, which propagate over thousands of kilometers southwestward toward the northern flank of the ACC.

Also, the dominance of one polarity goes along with the same polarity having larger mean amplitudes, somewhat larger diameters, larger intensities, and longer lifespans. In addition, eddies of the dominant polarity are typically formed more frequently. The causes for asymmetries of anticyclones and cyclones in these respects are subject to ongoing research [e.g., *Arai and Yamagata*, 1994; *Nycander*, 1994; *Cenedese and Linden*, 1999; *Hakim et al*., 2002; *Frisius*, 2003; *Graves et al*., 2006; *Ponomarev et al*., 2009; *Moisy et al*., 2011; *Perret et al*., 2011; *Badin*, 2013; *Heinloo et al*., 2012].

By analyzing the surface (satellite microwave based SST) and subsurface (Argo float profile temperatures and salinities) shape of eddies, we estimated the effect of eddies on tracers (Figure 1a). Based on the analysis of the surface imprint of eddies on temperature, we found eddies to act on tracers via a combination of *trapping*, which may imply nonlocal transport, and *stirring*, which is due to the rotation of eddies and results in a (more) local effect. *Trapping* is associated with the eddy's core and a monopole SST pattern, *stirring* with a dipole SST pattern along the eddy's periphery which is in continuous exchange with ambient waters (see also modeling study by *Early et al*. [2011]). We draw these conclusions from the shape of the SST anomalies, which can be explained as a superposition of a monopole and dipole pattern, and the colocation of closed SST contours associated with the eddy core.

Temperature, salinity, and density anomalies of eddies reach down to 2000 m, i.e., down to the deepest depth we have data available. Below the mixed layer at intermediate depth (approximately down to 1000 m), the stratification (layer thickness) of eddies and vertical gradients of temperature and salinity are clearly different from neighboring waters, indicating isopycnal advection, with possible contribution by downward diapycnal mixing of the near-surface anomaly. Below 1000–1500 m temperature and salinity anomalies can likely be explained largely by adiabatic heaving (cyclones) and suppressing (anticyclones) of isopycnals, which compensate upper ocean density anomalies.

Our results suggest that the variance of the SST anomaly of eddies is largely determined by *trapping*, with some eddies north of the ACC showing a major contribution due to *stirring*. However, as eddy swirl velocities are larger than cross-frontal eddy propagation velocities, the heat transport associated with *stirring* is dominant in the upper ocean. Eddy propagation velocities are constant throughout depth whereas swirl velocities decrease with depth, in accordance with depth-decreasing eddy density anomalies, which supposedly results in a column integrated heat transport (instead of mixed layer only) with a larger contribution by *trapping*. Transport due to *trapping* remains uncertain, first as the propagation velocity appropriate to use in the transport calculation is unclear (see e.g., differences between *Hausmann and Czaja* [2012] and *Dong et al*. [2014]), and second as the ability and extent eddies are able to trap fluid is a topical field of research.

The potential caveat of this work is that results that are dependent on lifetime properties of eddies, such as migration distances or nurseries and graveyards, are dependent on the tracking algorithm, which is subjective to some extent (e.g., eddies frequently split and merge). Eddy tracking is difficult in the highly dynamic areas where eddies frequently interact. Likewise we cannot exclude a bias with respect to propagation properties, nurseries and graveyards of eddies and their lifespans. Having said that, we believe the tendencies of our results to be robust.

There are implications of our findings: eddies are frequently investigated in terms of eddy kinetic energy. This approach typically does not differentiate polarity. Dependent on the question posed, it can be important to consider the inhomogeneous distribution of anticyclones and cyclones. We note that one cannot determine an eddy's polarity by solely relying on SST information, which is of importance for SST-based eddy detection [see also *Chaigneau et al*., 2011].

Trapping is not explicitly accounted for in parametrizations of eddies in coarse resolution numerical models. In future work, it could be useful to relate eddy properties as derived in this work to the *trapping* efficiencies of eddies as a step toward a parameterization of this effect. Potential approaches to assess the *trapping* efficiency of eddies could be based on the recent work by *Haller and Beron-Vera* [2013] and *Beron-Vera et al*.

[2013] (detection of impermeable eddies) or by seeding eddies with particles or release a dye tracer to "empirically" assessing the leakage [*Donners and Drijfhout*, 2004; *Nakano et al*., 2013]. Next to the *trapping* efficiency, the spatial scale of this effect is important for the development of a parameterization. Or for instance, if most eddies propagate only 10–100 km in most regions the effect might not need an additional parameterization even if they trapped perfectly.

A final comment on the "custom" to discard "short-lived" eddies from analyses with the reasoning that they might be spurious features (if the analysis is based on satellite data). The lifespan distribution drops off steeply with longer lifespans. Even if long-lived eddies, such as Agulhas rings may be prominent features and cause significant nonlocal transports, short-lived eddies form the majority and may be essential for integrated eddy effects, such as mixing. That is, it may be misleading to consider mainly long-lived distinct features in analyses such as heat transports. If short-lived eddies are non-negligible, including them in analyses may decrease the gap of Eulerian-based and Lagrangian-based eddy transport estimates as found for instance by *Treguier et al*. [2003].

Acknowledgments

The altimeter products used for this study were produced by Ssalto/Duacs and distributed by Aviso, with support from Cnes (http://www.aviso.oceanobs.com/duacs/). The SST data are produced by Remote Sensing Systems and sponsored by the NASA Ocean Vector Winds Science Team. Data are available at http://www.remss.com. The profiling float data data were collected and made freely available by the International Argo Program and the national programs that contribute to it (http://www.Argo.ucsd.edu, http://Argo.jcommops.org). The Argo Program is part of the Global Ocean Observing System. The eddy data set which was created in this study and used to produce the figures of this article is available from the authors upon request. The Center for Climate Systems Modelling (C2SM) at ETH Zurich and the Swiss National Science Foundation (grant P2EZP2-152133) provided financial support for this project. We thank Bridget Zakrzewski for insights on regional variations of subsurface properties of Southern Ocean eddies, and Stephen Griffies, David Byrne, and Ryan Abernathey for helpful comments.

References

Abernathey, R., J. Marshall, M. Mazloff, and E. Shuckburgh (2010), Enhancement of mesoscale eddy stirring at steering levels in the Southern Ocean, *J. Phys. Oceanogr.*, *40*, 170–184, doi:10.1175/2009JPO4201.1.

Adams, D. K., D. J. McGillicuddy, L. Zamudio, A. M. Thurnherr, X. Liang, O. Rouxel, C. R. German, and L. S. Mullineaux (2011), Surface-generated mesoscale eddies transport deep-sea products from hydrothermal vents, *Science*, *332*(6029), 580–583, doi:10.1126/science.1201066.

Ansorge, I., J. Jackson, K. Reid, J. Durgadoo, S. Swart, and S. Eberenz (2014), Evidence of a southward eddy corridor in the south-west Indian ocean, *Deep Sea Res., Part II*, *119*, 69–76, doi:10.1016/j.dsr2.2014.05.012.

Ansorge, I. J., E. A. Pakhomov, S. Kaehler, J. R. E. Lutjeharms, and J. V. Durgadoo (2009), Physical and biological coupling in eddies in the lee of the South-West Indian Ridge, *Polar Biol.*, *33*(6), 747–759, doi:10.1007/s00300-009-0752-9.

Arai, M., and T. Yamagata (1994), Asymmetric evolution of eddies in rotating shallow water, *Chaos*, *4*(2), 163–175, doi:10.1063/1.166001.

Arhan, M., X. Carton, A. Piola, and W. Zenk (2002), Deep lenses of circumpolar water in the Argentine Basin, *J. Geophys. Res.*, *107*(C1), 3007, doi:10.1029/2001JC000963.

Badin, G. (2013), Surface semi-geostrophic dynamics in the ocean, *Geophys. Astrophys. Fluid Dyn.*, *1075*(5), 526–540, doi:10.1080/03091929.2012.740479.

Bates, M., R. Tulloch, J. Marshall, and R. Ferrari (2014), Rationalizing the spatial distribution of mesoscale eddy diffusivity in terms of mixing length theory, *J. Phys. Oceanogr.*, *44*, 1523–1540, doi:10.1175/JPO-D-13-0130.1.

Beal, L. M., W. P. M. De Ruijter, A. Biastoch, and R. Zahn (2011), On the role of the Agulhas system in ocean circulation and climate, *Nature*, *472*, 429–436, doi:10.1038/nature09983.

Beron-Vera, F. J., Y. Wang, M. J. Olascoaga, G. J. Goni, and G. Haller (2013), Objective detection of oceanic eddies and the Agulhas Leakage, *J. Phys. Oceanogr.*, *43*, 1426–1438, doi:10.1175/JPO-D-12-0171.1.

Böning, C. W., A. Dispert, M. Visbeck, S. R. Rintoul, and F. U. Schwarzkopf (2008), The response of the Antarctic Circumpolar Current to recent climate change, *Nat. Geosci.*, *1*, 864–869, doi:10.1038/ngeo362.

Byrne, D., L. Papritz, I. Frenger, M. Münnich, and N. Gruber (2015), Atmospheric response to mesoscale sea surface temperature anomalies: Assessment of mechanisms and coupling strength in a high-resolution coupled model over the South Atlantic, *J. Atmos. Sci.*, *72*, 1872–1890, doi:10.1175/JAS-D-14-0195.1.

Carton, J. A., and B. S. Giese (2008), A reanalysis of ocean climate using simple ocean data assimilation (SODA), *Mon. Weather Rev.*, *136*(8), 2999–3017, doi:10.1175/2007MWR1978.1.

Casey, K. S., T. B. Brandon, P. Cornillon, R. Evans, V. Barale, J. Gower, and L. Alberotanza (2010), The past, present and future of the AVHRR Pathfinder SST program, in *Oceanography From Space*, edited by V. Barale, J. Gower, and L. Alberotanza, pp. 273–287, Springer, Dordrecht, Netherlands, doi:10.1007/978-90-481-8681-5.

Castelao, R. M. (2014), Mesoscale eddies in the South Atlantic Bight and the Gulf Stream Recirculation region: Vertical structure, *J. Geophys. Res. Oceans*, *119*, 2048–2065, doi:10.1002/2014JC009796.

Cenedese, C., and P. F. Linden (1999), Cyclone and anticyclone formation in a rotating stratified fluid over a sloping bottom, *J. Fluid Mech.*, *381*, 199–223, doi:10.1017/S0022112098003644.

Chaigneau, A., A. Gizolme, and C. Grados (2008), Mesoscale eddies off Peru in altimeter records: Identification algorithms and eddy spatio-temporal patterns, *Prog. Oceanogr.*, *79*(2–4), 106–119, doi:10.1016/j.pocean.2008.10.013.

Chaigneau, A., G. Eldin, and B. Dewitte (2009), Eddy activity in the four major upwelling systems from satellite altimetry (1992–2007), *Prog. Oceanogr.*, *83*(1–4), 117–123, doi:10.1016/j. pocean.2009.07.012.

Chaigneau, A., M. Le Texier, G. Eldin, C. Grados, and O. Pizarro (2011), Vertical structure of mesoscale eddies in the eastern South Pacific Ocean: A composite analysis from altimetry and Argo profiling floats, *J. Geophys. Res.*, *116*, C11025, doi:10.1029/2011JC007134.

Chelton, D. B., M. G. Schlax, D. L. Witter, and J. G. Richman (1990), Geosat altimeter observations of the surface circulation of the Southern Ocean, *J. Geophys. Res.*, *95*(C10), 17,877–17,903, doi:10.1029/JC095iC10p17877.

Chelton, D. B., R. A. DeSzoeke, M. G. Schlax, K. El Naggar, and N. Siwertz (1998), Geographical variability of the first baroclinic Rossby radius of deformation, *J. Phys. Oceanogr.*, *28*, 433–460, doi:10.1175/1520-0485(1998)028<0433:GVOTFB>2.0.CO;2.

Chelton, D. B., M. G. Schlax, R. M. Samelson, and R. A. de Szoeke (2007), Global observations of large oceanic eddies, *Geophys. Res. Lett.*, *34*, L15606, doi:10.1029/2007GL030812.

Chelton, D. B., P. Gaube, M. G. Schlax, J. J. Early, and R. M. Samelson (2011a), The influence of nonlinear mesoscale eddies on near-surface oceanic chlorophyll, *Science*, *334*(6054), 328–332, doi:10.1126/science.1208897.

Chelton, D. B., M. G. Schlax, and R. M. Samelson (2011b), Global observations of nonlinear mesoscale eddies, *Prog. Oceanogr.*, *91*, 167–216, doi:10.1016/j.pocean.2011.01.002.

Cushman-Roisin, B., and J.-M. Beckers (2011), Fronts, jets and vortices, in *Introduction to Geophysical Fluid Dynamics—Physical and Numerical Aspects, International Geophysics*, vol. 101, chap. 18, pp. 589–623, Elsevier, Oxford, U. K., doi:10.1016/B978-0-12-088759-0.00018-3.

Cushman-Roisin, B., E. P. Chassignet, and B. Tang (1989), Westward motion of mesoscale eddies, *J. Phys. Oceanogr.*, *20*, 758–768.
De Steur, L., and P. van Leeuwen (2009), The influence of bottom topography on the decay of modeled Agulhas rings, *Deep Sea Res., Part I*, *56*(4), 471–494, doi:10.1016/j.dsr.2008.11.009.
De Szoeke, R. A., and M. D. Levine (1981), The advective flux of heat by mean geostrophic motions in the Southern Ocean, *Deep Sea Res., Part A*, *28*(10), 1057–1085, doi:10.1016/0198-0149(81)90048-0.
Dencausse, G., M. Arhan, and S. Speich (2010), Routes of Agulhas rings in the southeastern Cape Basin, *Deep Sea Res., Part I*, *57*(11), 1406–1421, doi:10.1016/j.dsr.2010.07.008.
Dong, C., F. Nencioli, Y. Liu, and J. C. McWilliams (2011), An automated approach to detect oceanic eddies from satellite remotely sensed sea surface temperature data, *IEEE Geosci. Remote Sens. Lett.*, *8*(6), 1055–1059, doi:10.1109/LGRS.2011.2155029.
Dong, C., J. C. McWilliams, Y. Liu, and D. Chen (2014), Global heat and salt transports by eddy movement, *Nat. Commun.*, *5*, 3294, doi:10.1038/ncomms4294.
Donners, J., and S. Drijfhout (2004), Impact of cooling on the water mass exchange of Agulhas rings in a high resolution ocean model, *Geophys. Res. Lett.*, *31*, L16312, doi:10.1029/2004GL020644.
D'Ovidio, F., J. Isern-Fontanet, C. López, E. Hernández-García, and E. García-Ladona (2009), Comparison between Eulerian diagnostics and finite-size Lyapunov exponents computed from altimetry in the Algerian basin, *Deep Sea Res., Part I*, *56*(1), 15–31, doi:10.1016/j.dsr.2008.07.014.
Early, J. J., R. M. Samelson, and D. B. Chelton (2011), The evolution and propagation of quasigeostrophic ocean eddies, *J. Phys. Oceanogr.*, *41*, 1535–1555, doi:10.1175/2011JPO4601.1.
Everett, J. D., M. E. Baird, P. R. Oke, and I. M. Suthers (2012), An avenue of eddies: Quantifying the biophysical properties of mesoscale eddies in the Tasman Sea, *Geophys. Res. Lett.*, *39*, L16608, doi:10.1029/2012GL053091.
Faghmous, J. H., L. Styles, V. Mithal, S. Boriah, S. Liess, V. Kumar, F. Vikebo, and M. D. S. Mesquita (2012), EddyScan: A physically consistent ocean eddy monitoring application, in *Proc. Conf. Intel. Data Under.*, pp. 96–103, IEEE, Boulder, Colo., doi:10.1109/CIDU.2012.6382189. [Available at http://ieeexplore.ieee.org/xpls/abs_all.jsp?arnumber=6382189&tag=1.]
Fernandes, A. M., S. Nascimento, and D. Boutov (2011), Automatic identification of oceanic eddies in infrared satellite images, *Comput. Geosci.*, *37*(11), 1783–1792, doi:10.1016/j.cageo.2010.12.007.
Ferrari, R. (2011), Ocean science. A frontal challenge for climate models, *Science*, *332*(6027), 316–317, doi:10.1126/science.1203632.
Ferrari, R., and M. Nikurashin (2010), Suppression of eddy diffusivity across jets in the Southern Ocean, *J. Phys. Oceanogr.*, *40*, 1501–1519, doi:10.1175/2010JPO4278.1.
Ferrari, R., and C. Wunsch (2009), Ocean circulation kinetic energy: Reservoirs, sources, and sinks, *Annu. Rev. Fluid Mech.*, *41*, 253–282, doi:10.1146/annurev.fluid.40.111406.102139.
Flierl, G. G. R. (1981), Particle motions in large-amplitude wave fields, *Geophys. Astrophys. Fluid Dyn.*, *18*(1–2), 39–74, doi:10.1080/03091928108208773.
Frenger, I. (2013), On Southern Ocean eddies and their impacts on biology and the atmosphere, PhD thesis, ETH Zurich, Zurich, Switzerland, doi:10.3929/ethz-a-009938120.
Frenger, I., N. Gruber, R. Knutti, and M. Münnich (2013), Imprint of Southern Ocean eddies on winds, clouds and rainfall, *Nat. Geosci.*, *6*, 608–612, doi:10.1038/ngeo1863.
Frisius, T. (2003), The development of a cyclone-anticyclone asymmetry within a growing baroclinic wave, *J. Atmos. Sci.*, *60*, 2887–2906, doi:10.1175/1520-0469(2003)060<2887:TDOACA>2.0.CO;2.
Frölicher, T., J. Sarmiento, D. Paynter, J. Dunne, and M. Winton (2015), Anthropogenic carbon and heat uptake in CMIP5 models: The dominance of the Southern Ocean, *J. Clim.*, *28*, 862–886, doi:10.1175/JCLI-D-14-00117.1.
Fu, L.-L. (2009), Pattern and velocity of propagation of the global ocean eddy variability, *J. Geophys. Res.*, *114*, C11017, doi:10.1029/2009JC005349.
Fyfe, J. C., and O. A. Saenko (2006), Simulated changes in the extratropical Southern Hemisphere winds and currents, *Geophys. Res. Lett.*, *33*, L06701, doi:10.1029/2005GL025332.
Gent, P. R. (2011), The Gent-McWilliams parameterization: 20/20 hindsight, *Ocean Modell.*, *39*(1–2), 2–9, doi:10.1016/j.ocemod.2010.08.002.
Gent, P. R., J. Willebrand, T. J. McDougall, and J. C. McWilliams (1995), Parameterizing eddy-induced tracer transports in ocean circulation models, *J. Phys. Oceanogr.*, *25*, 463–474, doi:10.1175/1520-0485(1995)025<0463:PEITTI>2.0.CO;2.
Gille, S. T. (2003), Float observations of the Southern Ocean. Part I: Estimating mean fields, bottom velocities, and topographic steering, *J. Phys. Oceanogr.*, *33*, 1167–1181, doi:10. 1175/1520-0485(2003)033<1167:FOOTSO>2.0.CO;2.
Gille, S. T., E. J. Metzger, and R. Tokmakian (2004), Seafloor topography and ocean circulation, *Oceanography*, *17*(1), 47–54, doi:10.5670/oceanog.2004.66.
Gillett, N. P., D. A. Stone, P. A. Stott, T. Nozawa, A. Y. Karpechko, G. C. Hegerl, M. F. Wehner, and P. D. Jones (2008), Attribution of polar warming to human influence, *Nat. Geosci.*, *1*, 750–754, doi:10.1038/ngeo338.
Graves, L. P., J. C. McWilliams, and M. T. Montgomery (2006), Vortex evolution due to straining: A mechanism for dominance of strong, interior anticyclones, *Geophys. Astrophys. Fluid Dyn.*, *100*, 151–183, doi:10.1080/03091920600792041.
Griffa, A., R. Lumpkin, and M. Veneziani (2008), Cyclonic and anticyclonic motion in the upper ocean, *Geophys. Res. Lett.*, *35*, L01608, doi:10.1029/2007GL032100.
Griffies, S. M., et al. (2015), Impacts on ocean heat from transient mesoscale eddies in a hierarchy of climate models, *J. Clim.*, *28*, 952–977, doi:10.1175/JCLI-D-14-00353.1.
Gruber, N., Z. Lachkar, H. Frenzel, P. Marchesiello, M. Münnich, J. C. McWilliams, T. Nagai, and G.-K. Plattner (2011), Eddy-induced reduction of biological production in eastern boundary upwelling systems, *Nat. Geosci.*, *4*, 787–792, doi:10.1038/ngeo1273.
Hakim, G. J., C. Snyder, and D. J. Muraki (2002), A new surface model for cyclone-anticyclone asymmetry, *J. Atmos. Sci.*, *59*, 2405–2420, doi:10.1175/1520-0469(2002)059<2405:ANSMFC>2.0.CO;2.
Hallberg, R. (2013), Using a resolution function to regulate parameterizations of oceanic mesoscale eddy effects, *Ocean Modell.*, *72*, 92–103, doi:10.1016/j.ocemod.2013.08.007.
Hallberg, R., and A. Gnanadesikan (2006), The role of eddies in determining the structure and response of the wind-driven southern hemisphere overturning: Results from the modeling eddies in the Southern Ocean (MESO) Project, *J. Phys. Oceanogr.*, *36*, 2232–2252, doi:10.1175/JPO2980.1.
Haller, G., and F. J. Beron-Vera (2013), Coherent Lagrangian vortices: The black holes of turbulence, *J. Fluid Mech.*, *731*, R4, doi:10.1017/jfm.2013.391.
Hausmann, U., and A. Czaja (2012), The observed signature of mesoscale eddies in sea surface temperature and the associated heat transport, *Deep Sea Res., Part I*, *70*, 60–72, doi:10.1016/j.dsr.2012.08.005.

Heinloo, J., A. Toompuu, and M.-J. Lilover (2012), Gyration effect of the large-scale turbulence in the upper ocean, *Environ. Fluid Mech.*, *12*(5), 429–438, doi:10.1007/s10652-012-9247-2.
Henson, S. A., and A. C. Thomas (2008), A census of oceanic anticyclonic eddies in the Gulf of Alaska, *Deep Sea Res., Part I*, *55*(2), 163–176, doi:10.1016/j.dsr.2007.11.005.
Hogg, A. M., and J. R. Blundell (2006), Interdecadal variability of the Southern Ocean, *J. Phys. Oceanogr.*, *36*, 1626–1645, doi:10.1175/JPO2934.1.
Hogg, A. M., M. P. Meredith, J. R. Blundell, and C. Wilson (2008), Eddy heat flux in the Southern Ocean: Response to variable wind forcing, *J. Clim.*, *21*, 608–620, doi:10.1175/2007JCLI1925.1.
Isern-Fontanet, J., E. García-Ladona, and J. Font (2003), Identification of marine eddies from altimetric maps, *J. Atmos. Oceanic Technol.*, *20*, 772–778, doi:10.1175/1520-0426(2003)20<772:IOMEFA>2.0.CO;2.
Isern-Fontanet, J., E. García-Ladona, and J. Font (2006), Vortices of the Mediterranean Sea: An altimetric perspective, *J. Phys. Oceanogr.*, *36*, 87–103, doi:10.1175/JPO2826.1.
Itoh, S., and I. Yasuda (2010), Characteristics of mesoscale eddies in the Kuroshio-Oyashio extension region detected from the distribution of the sea surface height anomaly, *J. Phys. Oceanogr.*, *40*(5), 1018–1034, doi:10.1175/2009JPO4265.1.
Ivchenko, V., S. Danilov, and D. Olbers (2008), Eddies in numerical models of the Southern Ocean, in *Ocean Modeling in an Eddying Regime*, edited by M. W. Hecht and H. Hasumi, AGU, Washington, D. C., doi:10.1029/177GM13.
Jayne, S. R., and J. Marotzke (2002), The oceanic eddy heat transport, *J. Phys. Oceanogr.*, *32*, 3328–3345, doi:10.1175/1520-0485(2002)032<3328:TOEHT>2.0.CO;2.
Johnson, G. C., and H. L. Bryden (1989), On the size of the Antarctic Circumpolar Current, *Deep Sea Res., Part A*, *36*(1), 39–53, doi:10.1016/0198-0149(89)90017-4.
Kelly, K. A., R. C. Beardsley, R. Limeburner, K. H. Brink, J. D. Paduan, and T. K. Chereskin (1998), Variability of the near-surface eddy kinetic energy in the California Current based on altimetric, drifter, and moored current data, *J. Geophys. Res.*, *103*(C6), 13,067–13,083, doi:10.1029/97JC03760.
Klocker, A., and R. Abernathey (2014), Global patterns of mesoscale eddy properties and diffusivities, *J. Phys. Oceanogr.*, *44*, 1030–1046, doi:10.1175/JPO-D-13-0159.1.
Kurczyn, J. A., E. Beier, M. F. Lavín, and A. Chaigneau (2012), Mesoscale eddies in the northeastern Pacific tropical-subtropical transition zone: Statistical characterization from satellite altimetry, *J. Geophys. Res.*, *117*, C10021, doi:10.1029/2012JC007970.
Lachkar, Z., J. C. Orr, J.-C. Dutay, and P. Delecluse (2007), Effects of mesoscale eddies on global ocean distributions of CFC-11, CO_2, and δ14C, *Ocean Sci.*, *3*, 461–482.
Le Quéré, C., et al. (2007), Saturation of the Southern Ocean CO_2 sink due to recent climate change, *Science*, *316*(5832), 1735–1738, doi:10.1126/science.1136188.
Lehahn, Y., F. D'Ovidio, M. Lévy, Y. Amitai, and E. Heifetz (2011), Long range transport of a quasi isolated chlorophyll patch by an Agulhas ring, *Geophys. Res. Lett.*, *38*, L16610, doi:10.1029/2011GL048588.
Liang, J.-H., J. C. McWilliams, J. Kurian, F. Colas, P. Wang, and Y. Uchiyama (2012), Mesoscale variability in the northeastern tropical Pacific: Forcing mechanisms and eddy properties, *J. Geophys. Res.*, *117*, C07003, doi:10.1029/2012JC008008.
Liang, X., and A. M. Thurnherr (2012), Eddy-modulated internal waves and mixing on a midocean ridge, *J. Phys. Oceanogr.*, *42*, 1242–1248, doi:10.1175/JPO-D-11-0126.1.
Liu, Y., C. Dong, Y. Guan, D. Chen, J. McWilliams, and F. Nencioli (2012), Eddy analysis in the subtropical zonal band of the North Pacific Ocean, *Deep Sea Res., Part I*, *68*, 54–67, doi:10.1016/j.dsr.2012.06.001.
Lovenduski, N. S., N. Gruber, and S. C. Doney (2008), Toward a mechanistic understanding of the decadal trends in the Southern Ocean carbon sink, *Global Biogeochem. Cycles*, *22*, GB3016, doi:10.1029/2007GB003139.
Marshall, J., and T. Radko (2003), Residual-mean solutions for the Antarctic Circumpolar Current and its associated overturning circulation, *J. Phys. Oceanogr.*, *33*, 2341–2354, doi:10.1175/1520-0485(2003)033<2341:RSFTAC>2.0.CO;2.
Marshall, J., and K. Speer (2012), Closure of the meridional overturning circulation through Southern Ocean upwelling, *Nat. Geosci.*, *5*, 171–180, doi:10.1038/ngeo1391.
Massey, F. (1951), The Kolmogorov-Smirnov test for goodness of fit, *J. Am. Stat. Assoc.*, *46*(253), 68–78, doi:10.2307/2280095.
Maximenko, N., M. Niler, P. Rio, O. Melnichenko, L. Centurioni, D. Chambers, V. Zlotnicki, and B. Galperin (2009), Mean dynamic topography of the ocean derived from satellite and drifting buoy data using three different techniques, *J. Atmos. Oceanic Technol.*, *26*, 1910–1919, doi:10.1175/2009JTECHO672.1.
McDougall, T. J., and P. M. Barker (2011), *Getting started with TEOS-10 and the Gibbs Seawater (GSW) Oceanographic Toolbox*, 28 pp., SCOR/IAPSO WG127.
McGillicuddy, D. J., A. R. Robinson, D. A. Siegel, H. W. Jannasch, R. Johnson, T. D. Dickey, J. McNeil, A. F. Michaels, and A. H. Knap (1998), Influence of mesoscale eddies on new production in the Sargasso Sea, *Nature*, *394*, 263–266, doi:10.1038/28367.
McWilliams, J. C. (2008), The nature and consequences of oceanic eddies, in *Ocean Modeling in an Eddying Regime*, edited by M. W. Hecht and H. Hasumi, AGU, Washington, D. C., doi:10.1029/177GM03.
Mignone, B. K., A. Gnanadesikan, J. L. Sarmiento, and R. D. Slater (2006), Central role of Southern Hemisphere winds and eddies in modulating the oceanic uptake of anthropogenic carbon, *Geophys. Res. Lett.*, *33*, L01604, doi:10.1029/2005GL024464.
Mikaloff Fletcher, S. E., et al. (2006), Inverse estimates of anthropogenic CO_2 uptake, transport, and storage by the ocean, *Global Biogeochem. Cycles*, *20*, GB2002, doi:10.1029/2005GB002530.
Moisy, F., C. Morize, M. Rabaud, and J. Sommeria (2011), Decay laws, anisotropy and cyclone-anticyclone asymmetry in decaying rotating turbulence, *J. Fluid Mech.*, *666*, 5–35, doi:10.1017/S0022112010003733.
Morrison, A. K., and A. M. Hogg (2012), On the relationship between Southern Ocean overturning and ACC transport, *J. Phys. Oceanogr.*, *43*, 140–148, doi:10.1175/JPO-D-12-057.1.
Morrison, A. K., O. A. Saenko, A. M. Hogg, and P. Spence (2013), The role of vertical eddy flux in Southern Ocean heat uptake, *Geophys. Res. Lett.*, *40*, 5445–5450, doi:10.1002/2013GL057706.
Morrow, R. (2004), Divergent pathways of cyclonic and anti-cyclonic ocean eddies, *Geophys. Res. Lett.*, *31*, L24311, doi:10.1029/2004GL020974.
Morrow, R., and P.-Y. Le Traon (2012), Recent advances in observing mesoscale ocean dynamics with satellite altimetry, *Adv. Space Res.*, *50*(8), 1062–1076, doi:10.1016/j.asr.2011.09.033.
Nakano, H., H. Tsujino, and K. Sakamoto (2013), Tracer transport in cold-core rings pinched off from the Kuroshio Extension in an eddy-resolving ocean general circulation model, *J. Geophys. Res. Oceans*, *118*, 5461–5488, doi:10.1002/jgrc.20375.

Naveira Garabato, A. C., K. L. Polzin, B. A. King, K. J. Heywood, and M. Visbeck (2004), Widespread intense turbulent mixing in the Southern Ocean, *Science*, *303*(5655), 210–213, doi:10.1126/science.1090929.
Naveira Garabato, A. C., R. Ferrari, and K. L. Polzin (2011), Eddy stirring in the Southern Ocean, *J. Geophys. Res.*, *116*, C09019, doi:10.1029/2010JC006818.
Neu, U., et al. (2013), IMILAST—A community effort to intercompare extratropical cyclone detection and tracking algorithms: Assessing method-related uncertainties, *Bull. Am. Meteorol. Soc.*, *94*, 529–547, doi:10.1175/BAMS-D-11-00154.1.
Nikurashin, M., G. K. Vallis, and A. Adcroft (2013), Routes to energy dissipation for geostrophic flows in the Southern Ocean, *Nat. Geosci.*, *6*, 48–51, doi:10.1038/ngeo1657.
Nycander, J. (1994), Steady vortices in plasmas and geophysical flows, *Chaos*, *4*, 253–267, doi:10.1063/1.166006.
Oh, I. S., and V. Zhurbas (2000), Study of spatial spectra of horizontal turbulence in the ocean using drifter data, *J. Phys. Oceanogr.*, *30*, 1790–1801, doi:10.1175/1520-0485(2000)030<1790:SOSSOH>2.0.CO;2.
Okubo, A. (1970), Horizontal dispersion of floatable particles in the vicinity of velocity singularities such as convergences, *Deep Sea Res. Oceanogr. Abstr.*, *17*, 445–454, doi:10.1016/0011-7471(70)90059-8.
Oschlies, A. (2002), Can eddies make ocean deserts bloom?, *Global Biogeochem. Cycles*, *16*(4), 1106, doi:10.1029/2001GB001830.
Pascual, A., Y. Faugere, G. Larnicol, and P.-Y. Le Traon (2006), Improved description of the ocean mesoscale variability by combining four satellite altimeters, *Geophys. Res. Lett.*, *33*, L02611, doi:10.1029/2005GL024633.
Pasquero, C., A. Provenzale, and A. Babiano (2001), Parameterization of dispersion in two-dimensional turbulence, *J. Fluid Mech.*, *439*, 279–303, doi:10.1017/S0022112001004499.
Penven, P., V. Echevin, J. Pasapera, F. Colas, and J. Tam (2005), Average circulation, seasonal cycle, and mesoscale dynamics of the Peru Current System: A modeling approach, *J. Geophys. Res.*, *110*, C10021, doi:10.1029/2005JC002945.
Perret, G., T. Dubos, and A. Stegner (2011), How large-scale and cyclogeostrophic barotropic instabilities favor the formation of anticyclonic vortices in the ocean, *J. Phys. Oceanogr.*, *41*, 303–328, doi:10.1175/2010JPO4362.1.
Petersen, M. R., S. J. Williams, M. E. Maltrud, M. W. Hecht, and B. Hamann (2013), A three-dimensional eddy census of a high-resolution global ocean simulation, *J. Geophys. Res. Oceans*, *118*, 1759–1774, doi:10.1002/jgrc.20155.
Ponomarev, V. M., A. A. Khapaev, and I. G. Yakushkin (2009), Nonlinear Ekman friction and asymmetry of cyclonic and anticyclonic coherent structures in geophysical flows, *Dokl. Earth Sci.*, *425*(2), 510–515, doi:10.1134/S1028334X09030362.
Redi, M. H. (1982), Oceanic isopycnal mixing by coordinate rotation, *J. Phys. Oceanogr.*, *12*, 1154–1158, doi:10.1175/1520-0485(1982)012<1154:OIMBCR>2.0.CO;2.
Ridgway, K. R., and J. R. Dunn (2007), Observational evidence for a Southern Hemisphere oceanic supergyre, *Geophys. Res. Lett.*, *34*(13), 1–5, doi:10.1029/2007GL030392.
Rintoul, S. R., C. W. Hughes, and D. Olbers (2001), The Antarctic Circumpolar Current system, in *Ocean Circulation and Climate*, edited by G. Siedler, J. Church, and J. Gould, pp. 271–302, Academic Press, London, U. K.
Robinson, A. R. (1983), *Eddies in Marine Science*, Springer, Berlin, doi:10.1007/978-3-642-69003-7.
Roemmich, D., G. C. Johnson, S. Riser, R. Davis, J. Gilson, W. B. Owens, S. L. Garzoli, and C. Schmid (2009), The Argo Program: Observing the global ocean with profiling floats, *Oceanography*, *22*(2), 34–43, doi:10.5670/oceanog.2009.36.
Sallée, J.-B., K. Speer, S. Rintoul, and S. Wijffels (2010), Southern Ocean thermocline ventilation, *J. Phys. Oceanogr.*, *40*, 509–529, doi:10.1175/2009JPO4291.1.
Sallée, J.-B. B., and S. R. Rintoul (2011), Parameterization of eddy-induced subduction in the Southern Ocean surface-layer, *Ocean Modell.*, *39*, 146–153, doi:10.1016/j.ocemod.2011.04.001.
Sallée, J. B., K. Speer, and R. Morrow (2008), Response of the Antarctic Circumpolar Current to atmospheric variability, *J. Clim.*, *21*, 3020–3039, doi:10.1175/2007JCLI1702.1.
Samelson, R. M., M. G. Schlax, and D. B. Chelton (2014), Randomness, symmetry, and scaling of mesoscale eddy life cycles, *J. Phys. Oceanogr.*, *44*, 1012–1029, doi:10.1175/JPO-D-13-0161.1.
Saraceno, M., and C. Provost (2012), On eddy polarity distribution in the southwestern Atlantic, *Deep Sea Res., Part I*, *69*, 62–69, doi:10.1016/j.dsr.2012.07.005.
Sarmiento, J. L., N. Gruber, M. A. Brzezinski, and J. P. Dunne (2004), High-latitude controls of thermocline nutrients and low latitude biological productivity, *Nature*, *427*, 56–60, doi:10.1038/nature02127.
Schonten, M. W., W. P. M. de Ruijter, P. J. van Leeuwen, and J. R. E. Lutjeharms (2000), Translation, decay and splitting of Agulhas rings in the southeastern Atlantic Ocean, *J. Geophys. Res.*, *105*(C9), 21,913–21,925, doi:10.1029/1999JC000046.
Shats, M., H. Xia, H. Punzmann, and G. Falkovich (2007), Suppression of turbulence by self-generated and imposed mean flows, *Phys. Rev. Lett.*, *99*(16), 164,502, doi:10.1103/PhysRevLett.99.164502.
Shuckburgh, E., G. Maze, D. Ferreira, J. Marshall, H. Jones, and C. Hill (2011), Mixed layer lateral eddy fluxes mediated by air-sea interaction, *J. Phys. Oceanogr.*, *41*, 130–144, doi:10.1175/2010JPO4429.1.
Siegel, D. A., P. Peterson, D. J. McGillicuddy, S. Maritorena, and N. B. Nelson (2011), Bio-optical footprints created by mesoscale eddies in the Sargasso Sea, *Geophys. Res. Lett.*, *38*, L13608, doi:10.1029/2011GL047660.
Sokolov, S., and S. R. Rintoul (2009a), Circumpolar structure and distribution of the Antarctic Circumpolar Current fronts: 2. Variability and relationship to sea surface height, *J. Geophys. Res.*, *114*, C11019, doi:10.1029/2008JC005248.
Sokolov, S., and S. R. Rintoul (2009b), Circumpolar structure and distribution of the Antarctic Circumpolar Current fronts: 1. Mean circumpolar paths, *J. Geophys. Res.*, *114*, C11018, doi:10.1029/2008JC005108.
Solomon, H. (1971), On the representation of isentropic mixing in ocean circulation models, *J. Phys. Oceanogr.*, *1*(3), 233–234, doi:10.1175/1520-0485(1971)001<0233:OTROIM>2.0.CO;2.
Speich, S., B. Blanke, P. de Vries, S. Drijfhout, K. Döös, A. Ganachaud, and R. Marsh (2002), Tasman leakage: A new route in the global ocean conveyor belt, *Geophys. Res. Lett.*, *29*(10), 55-1–55-4, doi:10.1029/2001GL014586.
Swart, N. C., I. J. Ansorge, and J. R. E. Lutjeharms (2008), Detailed characterization of a cold Antarctic eddy, *J. Geophys. Res.*, *113*, CO1009, doi:10.1029/2007JC004190.
Talley, L. (2013), Closure of the global overturning circulation through the Indian, Pacific, and Southern Oceans: Schematics and transports, *Oceanography*, *26*(1), 80–97, doi:10.5670/oceanog.2013.07.
Terry, P. W. (2000), Suppression of turbulence and transport by sheared flow, *Rev. Mod. Phys.*, *72*(1), 109–165, doi:10.1103/RevModPhys.72.109.
Thompson, A. F. (2008), The atmospheric ocean: Eddies and jets in the Antarctic Circumpolar Current, *Philos. Trans. R. Soc. A*, *366*(1885), 4529–4541, doi:10.1098/rsta.2008.0196.

Thompson, A. F., and J.-B. Sallée (2012), Jets and topography: Jet transitions and the impact on transport in the Antarctic Circumpolar Current, *J. Phys. Oceanogr.*, *42*, 956–972, doi:10.1175/JPO-D-11-0135.1.
Thompson, A. F., P. H. Haynes, C. Wilson, and K. J. Richards (2010), Rapid Southern Ocean front transitions in an eddy-resolving ocean GCM, *Geophys. Res. Lett.*, *37*, L23602, doi:10.1029/2010GL045386.
Thompson, K. R., and E. Demirov (2006), Skewness of sea level variability of the world's oceans, *J. Geophys. Res.*, *111*, C05005, doi:10.1029/2004JC002839.
Thoppil, P. G., J. G. Richman, and P. J. Hogan (2011), Energetics of a global ocean circulation model compared to observations, *Geophys. Res. Lett.*, *38*, L15607, doi:10.1029/2011GL048347.
Treguier, A., O. Boebel, B. Barnier, and G. Madec (2003), Agulhas eddy fluxes in a 1/6° Atlantic model, *Deep Sea Res., Part II*, *50*, 251–280, doi:10.1016/S0967-0645(02)00396-X.
Treguier, A., M. England, S. Rintoul, G. Madec, J. Le Sommer, and J.-M. Molines (2007), Southern Ocean overturning across streamlines in an eddying simulation of the Antarctic Circumpolar Current, *Ocean Sci.*, *3*, 491–507, doi:10.5194/osd-4-653-2007.
Treguier, A. M., J. Deshayes, J. Le Sommer, C. Lique, G. Madec, T. Penduff, J.-M. Molines, B. Barnier, R. Bourdalle-Badie, and C. Talandier (2014), Meridional transport of salt in the global ocean from an eddy-resolving model, *Ocean Sci.*, *10*, 243–255, doi:10.5194/os-10-243-2014.
Van Aken, H., A. van Veldhoven, C. Veth, W. de Ruijter, P. van Leeuwen, S. Drijfhout, C. Whittle, and M. Rouault (2003), Observations of a young Agulhas ring, Astrid, during MARE in March 2000, *Deep Sea Res., Part II*, *50*(1), 167–195, doi:10.1016/S0967-0645(02)00383-1.
Van Leeuwen, P. J. (2007), The propagation mechanism of a vortex on the β plane, *J. Phys. Oceanogr.*, *37*, 2316–2330, doi:10.1175/JPO3107.1.
Venaille, A., G. K. Vallis, and K. S. Smith (2011), Baroclinic turbulence in the ocean: Analysis with primitive equation and quasigeostrophic simulations, *J. Phys. Oceanogr*, *41*, 1605–1623, doi:10.1175/JPO-D-10-05021.1.
Volkov, D. L., T. Lee, and L.-L. Fu (2008), Eddy-induced meridional heat transport in the ocean, *Geophys. Res. Lett.*, *35*, L20601, doi:10.1029/2008GL035490.
Von Schuckmann, K., F. Gaillard, and P.-Y. Le Traon (2009), Global hydrographic variability patterns during 2003–2008, *J. Geophys. Res.*, *114*, C09007, doi:10.1029/2008JC005237.
Walkden, G. J., K. J. Heywood, and D. P. Stevens (2008), Eddy heat fluxes from direct current measurements of the Antarctic Polar Front in Shag Rocks Passage, *Geophys. Res. Lett.*, *35*, L06602, doi:10.1029/2007GL032767.
Weiss, J. (1991), The dynamics of enstrophy transfer in two-dimensional hydrodynamics, *Phys. D: Nonlinear Phenomena*, *48*(2–3), 273–294, doi:10.1016/0167-2789(91)90088-Q.
Whalen, C. B., L. D. Talley, and J. A. MacKinnon (2012), Spatial and temporal variability of global ocean mixing inferred from Argo profiles, *Geophys. Res. Lett.*, *39*, L18612, doi:10.1029/2012GL053196.
Williams, S., M. Petersen, M. Hecht, M. Maltrud, J. Patchett, J. Ahrens, and B. Hamann (2012), Interface exchange as an indicator for eddy heat transport, *Comput. Graphics Forum*, *31*, 1125–1134, doi:10.1111/j.1467-8659.2012.03105.x.
Zhai, X., H. L. Johnson, and D. P. Marshall (2010), Significant sink of ocean-eddy energy near western boundaries, *Nat. Geosci.*, *3*, 608–612, doi:10.1038/ngeo943.
Zhang, Z., Y. Zhang, W. Wang, and R. X. Huang (2013), Universal structure of mesoscale eddies in the ocean, *Geophys. Res. Lett.*, *40*, 3677–3681, doi:10.1002/grl.50736.
Zhang, Z., W. Wang, and B. Qiu (2014a), Oceanic mass transport by mesoscale eddies, *Science*, *345*(6194), 322–324, doi:10.1126/science.1252418.
Zhang, Z., Y. Zhong, J. Tian, Q. Yang, and W. Zhao (2014b), Estimation of eddy heat transport in the global ocean from Argo data, *Acta Oceanol. Sin.*, *33*(1), 42–47, doi:10.1007/s13131-014-0421-x.
Zickfeld, K., J. C. Fyfe, O. A. Saenko, M. Eby, and A. J. Weaver (2007), Response of the global carbon cycle to human-induced changes in Southern Hemisphere winds, *Geophys. Res. Lett.*, *34*, L12712, doi:10.1029/2006GL028797.
Zika, J. D., et al. (2013), Vertical eddy fluxes in the Southern Ocean, *J. Phys. Oceanogr.*, *43*, 941–955, doi:10.1175/JPO-D-12-0178.1.

Erratum

In the originally published version of this manuscript, there was an error in Figure 7. Nautical was shown instead of Kilometers. Also in section 3.2, "the vicinity of the ACC (100 km)" should have read "the vicinity of the ACC (*O*(100) km)". And lastly, in section 3.3 "propagation distances over their entire lifetime of 67 (44) km" should have read "propagation distances over their entire lifetime of 124 (81) km". These errors have since been corrected, and this version may be considered the authoritative version of record.